JOURNAL OF MASS SPECTROMETRY, VOL. 31, 771–790 (1996)

Prediction of a Space Charge Induced Upper Molecular Mass Limit Towards Achieving Unit Mass Resolution in Fourier Transform Ion Cyclotron Resonance Mass Spectrometry

Dale W. Mitchell and Richard D. Smith†
Pacific Northwest National Laboratory, Environmental Molecular Sciences Laboratory, P.O. Box 999, M.S. P8-19, Richland, Washington 99352, USA

Cyclotron phase locking arises when two ion clouds have similar mass-to-charge ratios and a sufficiently large ion population such that the relative cyclotron dynamics are dominated by the mutual Coulomb E × B drift dynamics. Once two or more ion clouds are phase locked, a Fourier transform ion cyclotron resonance mass spectrometer cannot distinguish them by image current detection since the ion clouds have identical detected cyclotron frequencies. A simple analytical model, based on the assumption of rigid ion clouds, predicts that the maximum number of ions having equal charge states and closely spaced masses, which can be contained in two clouds before phase locking occurs, is proportional to their mass difference and to the square of the magnetic field strength divided by the molecular mass, $\Delta m(B/M)^2$, and is independent of the charge state. This molecular mass dependence establishes an upper molecular mass limit for resolving closely spaced peaks due to cyclotron phase locking. The rigid ion cloud model, supported by numerical simulations, demonstrates that phase locking causes the 1 Da spacing of the isotopic envelope for large molecules to be unresolvable past a high molecular mass limit (M_{max}). M_{max} is directly proportional to B and independent of the charge state for adjacent ion clouds with equal charge state. An order of magnitude estimate predicts that $M_{max} \approx 1 \times 10^4 B$ (in units of Da and Tesla), independent of charge state for peaks having a 1 Da spacing. This estimate concurs with present instrumental capabilities. Full three-dimensional numerical simulations on realistic ion clouds, which include the combined effects of internal and external ion cloud dynamics, Z-oscillation, linear dipolar excitation and trap potential anharmonicity, demonstrate the qualitative validity of the assumptions inherent in the rigid ion cloud model predictions.

KEYWORDS: Fourier transform mass spectrometry; ion cyclotron resonance; phase locking; space charge effects; isotope ratios

INTRODUCTION

Among the most important applications of Fourier transform ion cyclotron resonance (FT-ICR) mass spectrometry (MS) is its ability to weigh simultaneously the mass-to-charge (m/z) ratios of many different ionic species with high precision.[1,2] Of recent significance is the capability of FT-ICR to determine the charge state of large multiply charged species arising from electrospray ionization (ESI) by resolving the isotopic envelope at a nominal 1 Da or u resolution.[2–4] For this situation, the molecular mass is determined unambiguously, allowing a straightforward assignment of mass peaks in an otherwise complicated spectrum. This capability of FT-ICR has proven crucial in biological applications, especially for the correct interpretation of MS^n of larger molecules by ESI.[2–4]

If many different m/zs are simultaneously confined in the ICR trap,[5] Coulombic interactions among the ions may significantly influence the instrumental performance. These space charge effects include position-dependent frequency shifts, mode amplitude and frequency modulations, and phase locking.[6–13] For high ion density experiments, diocotron and collective fluid modes are important.[14–16] Imperfect electrostatic and magnetic fields, specifically trap potential anharmonicity and magnetic field inhomogeneity, introduce ion position-dependent detected cyclotron frequencies.

The central purpose of this paper is to demonstrate that cyclotron phase locking due to Coulombic interactions sets a maximum molecular mass limit in FT-ICR mass spectrometers for achieving unit mass resolution under most practical conditions. This molecular mass limit is directly proportional to magnetic field and independent of charge state for two masses which are adjacent isotopes belonging to the same charge state. One should not confuse the molecular mass limit described here with the well known critical m/z trap limit,[5] which is a single ion property not related to Coulombic interactions (although the radial space charge electric field may modify the m/z trap limit), and also note that other factors can conspire to prevent the phase locking molecular mass limit discussed here from being recognized.

† Author to whom correspondence should be addressed.

CCC 1076–5174/96/070771–20

Received 19 December 1995
Accepted 25 March 1996

Phase locking of cyclotron modes

Phase locking of the cyclotron modes for two ion clouds results when the relative cyclotron dynamics are dominated by the mutual $\mathbf{E} \times \mathbf{B}$ drift dynamics, where $\mathbf{E}$ is the Coulomb electric field (an ion cloud is defined here as a coherently moving ion ensemble of the same mass and charge). If the ion clouds are not phase locked, then the two clouds move in individual cyclotron orbits with two distinct cyclotron frequencies. For the situation where Coulomb interactions are negligible, the difference in cyclotron frequency is $\Delta\omega_c = B|q_1/m_1 - q_2/m_2|$ and the relative velocity is $\Delta\omega_c R_c$, where B, R_c, q and m are the magnetic field, cyclotron radius, ionic charge and mass, respectively. Each ion cloud receives an additional cyclotron velocity perturbation equal to $\mathbf{v_d} = -(\mathbf{E} \times \mathbf{B})/B^2$ due to the Coulomb electric field between ion clouds.[11] Under most conditions, the net effect of $\mathbf{v_d}$ is to introduce a slight modulation in the otherwise circular cyclotron orbit with period $\sim\Delta\omega_c^{-1}$ and to shift the cloud's frequencies. As the number of ions increases, the modulation amplitudes increase up to the point where the ion clouds undergo cyclotron phase locking. Thereafter, the ion clouds have the same detected cyclotron frequencies and are indistinguishable in a mass spectrum by image current detection of the cyclotron modes. Cyclotron phase locking is an experimental reality, having been reported in a number of studies.[8,12,13]

In order to understand the origin of cyclotron phase locking, consider first the simple model of two unexcited ($R_c = 0$) line charges (zero radii charged cylinders) which are separated by a distance s. It is easy to see that for this situation the line charges rotate about each other due to $\mathbf{E} \times \mathbf{B}$ drift with a frequency $\omega_d = E/sB$. Now, if the Coulombically interacting line charges with cyclotron frequency difference $\Delta\omega_c$ are excited to coherent cyclotron radii R_c, there is a competition between the Coulomb $\mathbf{E} \times \mathbf{B}$ drift and relative cyclotron motion. The $\mathbf{E} \times \mathbf{B}$ drift locks the line charges together while the relative cyclotron motion keeps them apart. An estimate of the locking condition valid for $R_c \gg s$ is provided by equating the time required for the ion clouds to pass each other due to their relative cyclotron motion (τ_{rel}) with the time required to complete one rotation period due to $\mathbf{E} \times \mathbf{B}$ drift (τ_d).[10,11] If $\tau_d > \tau_{rel}$, the ion clouds rotate in perturbed (modulated) cyclotron orbits with slightly shifted cyclotron frequencies. However, if $\tau_d < \tau_{rel}$, then the line charges may lock cyclotron modes.

Recently, we have studied phase locking in detail and have shown that the model of two interacting line charges can be extended to two initially overlapping charged cylinders by replacing the separation distance s by an effective separation distance s_{eff} which is proportional to the ion cloud radius.[11] In particular, two infinitely long charged cylinders with cloud radii ρ_c, cyclotron radii R_c, which are initially overlapping are phase locked if their cyclotron frequency difference satisfies the equation (all numbered equations are in MKS units)

$$\Delta\omega_c < \frac{N_1 q_1 + N_2 q_2}{2\pi^2 \varepsilon_0 L B R_c s_{eff}} \qquad (1)$$

where $\varepsilon_0 = 8.85 \times 10^{-12}$ F m^{-1} is the vacuum permittivity and $N_j q_j$ is the total charge contained in a length of the jth cylinder L m long. As an approximation valid for long cylindrical ion clouds (neglecting edge effects), $N_j q_j$ is the total charge contained in the jth ion cloud whose length $L \gg \rho_c$. Our earlier work derives $s_{eff} \approx 1.04\rho_c$ for cylindrical ion clouds by parameterization of Eqn (1) with numerical simulations.[11] Equation (1) is accurate assuming $R_c \gg \rho_c$. Good agreement is found[11] between predictions of Eqn (1), numerical simulations and previously published experimental data.

An interesting situation occurs if instead of cyclotron phase locking, the locking of magnetron modes is considered. One arrives at an identical expression for the magnetron locking condition as Eqn (1) with $\Delta\omega_c$ replaced by the difference in magnetron frequency between the two clouds $\Delta\omega_-$. Since $\Delta\omega_-$ is virtually independent of m/z, one concludes immediately that for pure coherent magnetron motion (no coherent cyclotron motion) only a modest space charge electric field is required to lock the magnetron modes of all m/zs, resulting in a single collective magnetron mode with the same magnetron frequency for all m/zs.

RESULTS AND DISCUSSION

An important prediction of Eqn (1) occurs when $q_1 = q_2 = q$ (e.g. same charge state). Since $\Delta\omega_c$ and the space charge induced $\mathbf{E} \times \mathbf{B}$ drift are both directly proportional to q in this case, Eqn (1) predicts that the phase locking threshold is independent of the charge of the ion when the two ion clouds have the same charge state. This prediction may be understood simply by considering that as q increases then $\Delta\omega_c$ increases. At first glance, an increase in $\Delta\omega_c$ makes phase locking less likely to occur; however, this increase is exactly compensated by a corresponding increase in the Coulomb electric field, which makes phase locking more likely to occur. Therefore, the phase locking threshold is independent of the charge state if the two ion clouds have equal charge state ions.

Recently, we have studied phase locking in two ion clouds which have either cylindrical or spherical shape.[11] Comparison with previously published experimental data demonstrates that the cylindrical ion cloud model predicted phase locking thresholds in reasonable agreement with experiment. Furthermore, spherical ion clouds are more likely to lock cyclotron modes than long cylindrical clouds with equal cloud radii and total number of ions. For this situation, the number density of the spherical ion clouds is larger by $0.75(L/\rho_c) \gg 1$ the density in the cylindrical clouds. Therefore, absolute (best case) limits are established with cylindrical ion clouds. Detailed results are presented here for cylindrical ion clouds. Final results are also given for spherically shaped ion clouds, without proof, in order to compare with predictions based on cylindrical clouds.[11]

If Eqn (1) is satisfied, then the two charged cylinders do not separate into two independent cyclotron modes, but instead evolve with a single collective cyclotron frequency and a collective relative $\mathbf{E} \times \mathbf{B}$ drift frequency. At phase locking the $\mathbf{E} \times \mathbf{B}$ drift entrains one ion cloud

to the second ion cloud. If two ion clouds with different m/z are phase locked, an FT-ICR mass spectrometer cannot resolve the two mass peaks since the perturbed cyclotron frequencies, which are the measured quantities, are identical at phase locking.

Now, consider two cylindrical ion clouds composed of ions with the same charge state ($q_1 = q_2$), separated by a small mass difference $\Delta m = |m_1 - m_2|$, and with $m_1 \approx m_2 \approx m \gg \Delta m$. For these limits, Eqn (1) predicts that the maximum total number of ions $N_{max} = N_1 + N_2$ before the two clouds phase lock is

$$N_{max} \approx 20.5\left(\frac{\varepsilon_0 L R_c \rho_c B^2 \Delta m}{m^2}\right) \quad (2)$$

N_{max} predicted by Eqn (2) compares well with numerical simulations of the exact equations of motion and with previously published experimental data.[11] An important prediction of Eqn (2) is that N_{max} is independent of the relative abundance of ions in each cloud. This is actually an approximation which is valid provided that $R_c \gg \rho_c$.

Two different research groups have carried out experiments estimating the number of ions required to lock cyclotron modes.[8,12] Diagnostics are not currently employed by the ICR community to measure accurately the ion cloud geometry and number density,[14–16] and therefore we have to make some approximations when comparing Eqn (2) with available experimental data. The ion cloud is assumed to extend the entire length of the ICR trap such that L equals the trap length. In addition, the cloud radius $\rho_c \approx 0.1$ cm is chosen to be equal to a typical value for the radius of the ionizing electron beam or beam of externally generated ions.

Naito and Inoue[8] have investigated cyclotron phase locking experimentally with CO^+ (m_1 27.9949 u) and $C_2H_4^+$ (m_2 28.0313 u) with the ratio $N_1:N_2 = 0.38:0.62$, cyclotron radius $R_c = 1$ cm, magnetic field $B = 1$ Tesla (T) and trap length 3.3 cm, determining that a minimum of $\sim 1 \times 10^6$ ions is required to lock cyclotron modes with these conditions. Putting $B = 1$ T, $m = 28$ u, $\Delta m = 0.036$ u, $R_c = 1$ cm, $L = 3.3$ cm and $\rho_c = 0.1$ cm in Eqn (2), we predict $N_{max} = 1.7 \times 10^6$ ions.

In addition, Huang *et al.*[12] have measured the number of ions required to lock cyclotron modes in experiments with CO^+ (m_1 27.9949 u) and N_2^+ (m_2 28.0056 u) measured in two different relative abundances, namely, equal relative abundance and $N_1:N_2$ in the ratio 0.28:0.72. Their experiments find that $N_{max} \approx (1 \pm 0.3) \times 10^6$ ions for both relative abundances.[12] These experiments were carried out with a 0.7 T magnetic field and a 5 cm long ICR trap. The post-excitation cyclotron radius was not reported. With $B = 0.7$ T, $m = 28$ u, $\Delta m = 0.011$ u, $L = 5$ cm, $R_c = 1$ cm and $\rho_c = 0.1$ cm in Eqn (2), we predict $N_{max} = 0.4 \times 10^6$ ions. The predictions of Eqn (2) compare reasonably well with available data (remember that ρ_c and R_c were not measured and no attempt was made here to 'fit' Eqn (2) to the data).

On the other hand, the theoretical point charge model of Naito and Inoue[8] (NI) makes predictions which break down in either the limit that one ion cloud has a relative abundance much greater than the other ion cloud (N_{max} approaches infinity) or that the ion clouds have equal relative abundance (N_{max} is too small). For example, using the parameters above for the data of Huang *et al.*,[12] the NI model predicts $N_{max} = 0.4 \times 10^6$ ions when $N_1:N_2 = 0.28:0.72$; however, the NI model predicts incorrectly $N_{max} = 0.001$ ions when N_1 and N_2 are equally abundant. Experimentally,[12] the number of ions required to lock modes is not too sensitive of the relative abundance of ions, in agreement with Eqn (2). We present numerical simulations and additional analytical theory which demonstrate that N_{max} is nearly independent of the relative abundance of ions in each cloud as long as the cyclotron radius is much greater than the ion cloud radius. In addition, the phase locking condition predicted by the NI model does not take into account the initial separation distance between point charges (or the cloud radius for finite sized ion clouds). Recent numerical simulations and analytical theory demonstrate that the phase locking condition for two point charges strongly depends on the initial separation distance.[11] Nonetheless, there are two important predictions of the NI model which are in agreement with our work. Both Eqn (2) and the NI model predict the same magnetic field dependence and charge independence of the phase locking threshold when the charge states are equal.

Upper molecular mass limit due to cyclotron phase locking

An expression equivalent to Eqn (2) for the phase locking threshold is alternatively obtained by solving for the maximum molecular mass (M_{max}) of the ions before phase locking occurs

$$M_{max} \approx 3.2B\sqrt{\frac{\varepsilon_0 L R_c \rho_c \Delta m}{N_{ave}}} \quad (3)$$

where $N_{ave} = (N_1 + N_2)/2$ is the average number of ions in two adjacent ion clouds. For an isotopic distribution, N_{ave} is the average of the number of ions in the most abundant isotope peak and its most abundant immediate neighbor.

The important prediction from this analysis is the existence of a high molecular mass limit in the ability of FT-ICR to weigh simultaneously masses separated by Δm. If $\Delta m = 1$ u, then M_{max} is the high molecular mass limit towards achieving 1 u resolution. The dependences on R_c, Δm, m, B and number of ions predicted by Eqns (2) and (3) are not an artifact of our use of cylindrical ion clouds since similar derivations employing spherical ion clouds, line charges or point charges yield the same dependences.[11]

Using reasonable ICR experimental parameters, $L = 5$ cm, $R_c = 1$ cm, $\rho_c = 0.1$ cm and $N_{ave} = 250$, with $\Delta m = 1$ u, then Eqn (3) yields $M_{max} \approx 1 \times 10^4 B$ (units in u and T). This order of magnitude estimate is consistent with available experimental information. For example, the highest reported molecular mass ions with barely resolved 1 u separated mass peaks are $\sim 67 \times 10^3$ Da (porcine serum albumin) using a $B = 6.2$ T FT-ICR mass spectrometer.[4] Similar isotopic resolution for albumin has been obtained in our laboratory with a 7 T instrument. Reducing N_{ave} from 250 to

100 ions increases M_{max} by a factor of 1.6. The most important prediction of Eqn (3) is that M_{max}, for ions belonging to the same charge state, is independent of the charge and directly proportional to B. It must be remembered that this prediction only relates to the best achievable resolution, and that other experimental considerations[17] (related to observation time of coherent cyclotron motion and cyclotron frequency drifting during detection) may prevent this performance from being realized. However, if M_{max} is exceeded, then the isotopic envelope is unresolvable by image charge detection, regardless of other experimental parameters and instrumental performance.

We should point out that under typical ESI conditions, the maximum molecular mass limit, M_{max}, described here is more relevant than the well known critical m/z trap limit.[5] The critical m/z trap limit (m/z_{crit}) is a single ion property which is widely used as a figure of merit for particular ICR trap geometries. In general, the radial Coulombic electric field modifies m/z_{crit}. An ion whose m/z exceeds m/z_{crit} is not confined at all. Specifically, m/z_{crit} is dependent on the trap potential harmonicity and magnetic field by the relation $m/z_{crit} = B^2/4\Gamma$, where Γ is determined for any trap geometry by an expansion of the trap potential Φ_{trap} about the trap's geometric center, along the trap z-axis (i.e. $\Phi_{trap}(z) \approx \text{constant} + \Gamma z^2 + \cdots$). For a trap of width d, potential V_t on the end-caps (plates or rings) with ground on all other electrodes, $m/z_{crit} = B^2d^2/(4V_tD_2)$, where D_2 is a dimensionless coefficient. As a common example, a 5 cm cubic ICR trap ($D_2 = 2.7737$), with $V_t = 1$ in a 3 T magnetic field, has $m/z_{crit} = 2 \times 10^5$ u. In contrast, $m_{max} \approx 1 \times 10^4 B \approx 3 \times 10^4$ Da, using the parameters given above. Therefore, for multiply charged species, which are the norm for high molecular mass (though relatively low m/z) ions generated by electrospray, m/z_{crit} is easily avoided and controllable (e.g. lower V_t or different trap geometry[5,18]); however, since M_{max} is charge independent, this is the crucial limit for ESI applications.

It is possible to put Eqn (3) into a form which does not depend on the ion cloud geometry. Substituting the average number density, defined as $n_{ave} = N_{ave}/\pi\rho_c{}^2L$, into Eqn (3) yields

$$M_{max} \approx gB\sqrt{\frac{\varepsilon_0 R_c \Delta m}{\rho_c n_{ave}}} \tag{4}$$

where g is a dimensionless constant dependent on the ion cloud geometry. In particular, $g = 1.8$ for infinitely long cylindrical clouds and $g = 3.3$ for spherical ion clouds (note that $n_{ave} = 3N_{ave}/4\pi\rho_c{}^3$ for spherical clouds).[11]

It is interesting to compare M_{max} for long cylindrical ion clouds with spherical clouds which have the same radius and total number of ions. For this situation, $M_{max}^{sphere} \approx 2(\rho_c/L)^{0.5}M_{max}^{cyl.}$. As a typical example, M_{max} for a 0.1 cm radius spherical ion cloud is $\sim 0.3M_{max}$ for a 5 cm long cylindrical cloud with the same radius and number of ions as the spherical cloud.

Compressing the ion cloud decreases M_{max} as the inverse square root of the number density. While increasing the number density has the substantial benefit of increasing the stability of the coherent cyclotron motion,[9] it also increases the likelihood of cyclotron phase locking, for the same reason. The maximum density that an ion distribution consisting of a single m/z can be compressed to is set by the Brillouin density limit[19] ($n_B = \varepsilon_0 B^2/2m$). The Brillouin limit combined with Eqn (4) determines the smallest value of M_{max} as a result of compressing the ion cloud to its maximum density. As an example, consider an experiment where two closely spaced masses $m \gg \Delta m$ are confined, then Eqn (4) with $n_{ave} = n_B/2$ reduces to $M_{max} = 4g^2\Delta m(R_c/\rho_c)$. With $\Delta m = 1$ u, $R_c/\rho_c = 10$, then M_{max} is just 130 and 435 u for cylindrical and spherical clouds, respectively, which have been compressed to their maximum density. It is clear that an ion cloud consisting of two close spaced masses should not be compressed to its Brillouin limit for high molecular mass applications.

Isobaric masses and adjacent charge states

In reality, many charge states are simultaneously present and, furthermore, the isotope peaks within each charge state can be composed of many isobaric masses whose spacing is $\Delta m \ll 1$ u. A hierarchy of different Δm and Δz values is the normal occurrence in most ESI applications. The high molecular mass limit for resolving isobaric masses within a single isotope peak is simply Eqn (3) or (4) with Δm equal to the mass difference between two adjacent isobaric masses of interest. For example, if the isobaric masses are separated by $\Delta m = 0.001$ u in an FT-ICR mass spectrometer with $B = 3$ T, $R_c = 1$ cm, $L = 5$ cm, $\rho_c = 0.1$ cm and $N_{ave} = 1000$ ions, then Eqn (3) predicts that these isobaric masses are unresolvable for molecular mass species exceeding $M_{max} \approx 500$ u. This upper estimate is in keeping with experimental trends which have resolved isobaric mass peaks for singly charged ions at m/z 269 separated by $\Delta m = 0.0011$ u.[13]

While the isotopic envelope of one charge state may not always be resolvable in an ESI mass spectrum, the charge states are much easier to resolve at a $\Delta z = 1$ spacing. Provided that the cyclotron frequency difference between two adjacent charge states is greater than the cyclotron frequency width of a single charge state's isotopic envelope (so that the isotopes of neighboring charge states are not overlapping), then Eqn (1) can be used to predict the maximum charge (z_{max}) before phase locking occurs between two cylindrical ion clouds which have the same mass m but different z. With $m_1 = m_2 = m$ and $z_1 \approx z_2 \approx z \gg \Delta z$, where $\Delta z = |z_1 - z_2|$ in Eqn (1), we obtain

$$z_{max} = 3.2B\sqrt{\frac{\varepsilon_0 LR_c\rho_c\Delta z}{N_{ave}/(m/z)}} \tag{5}$$

where z_{max} is the upper z limit towards resolving two adjacent charge states whose masses are equal. As an example, let $\Delta z = 1$, $N_{ave} = 250$, $L = 5$ cm, $R_c = 1$ cm, $\rho_c = 0.1$ cm and $m/z = 1500$ u; then $z_{max} \approx 300B$. Since $m/z = 1500$ u (a value chosen as a typical m/z for large biopolymer ions generated by ESI), then $m = 1500z_{max} \approx 45 \times 10^4 B$ (tesla) is the corresponding high molecular mass limit towards separating these adjacent charge states.

Numerical simulations of phase locking in two or more rigid ion clouds

Numerical simulations with two or more Coulombically interacting rigid ion clouds are used to test further the predictions of Eqn (2) [Eqn (3) is equivalent to Eqn (2)]. Every different m/z is modeled as a uniform charge density infinitely long cylinder aligned parallel to the homogeneous magnetic field $B\hat{\mathbf{z}}$. A cylindrical ion cloud is perhaps the simplest model for cloud geometry capable of yielding semi-quantitative agreement with experiment to many important space charge effects including frequency shifts and cyclotron phase locking.[11] Each ion cloud (charged cylinder) has a radius ρ_c, and is allowed to interact with the Coulomb electric field from all other ion clouds in addition to the magnetic field and any externally applied electric fields. The dynamics of each ion cloud in the xy plane is solved by numerical integration of the equations of motion. The full three-dimensional simulation of realistic deformable ion clouds is carried out in later sections.

For a single ion (or the center position of an ion cloud), the magnetron and cyclotron motions in the quadrupole approximation can be separated from each other. The cyclotron and magnetron position vectors $\mathbf{r}_+$ and $\mathbf{r}_-$ for a single ion in the presence of a perturbing force $\mathbf{F}$ are given by the dynamic equation[11]

$$\frac{d\mathbf{r}_\pm}{dt} = \left[\omega_\pm \mathbf{r}_\pm \mp \frac{\mathbf{F}}{m(\omega_+ - \omega_-)}\right] \times \hat{\mathbf{z}} \qquad (6)$$

The ion's position in the xy plane is $\mathbf{r} = \mathbf{r}_+ + \mathbf{r}_-$. These equations reduce to the quadrupole approximation (i.e. an ion in an azimuthally symmetric quadratic electrostatic potential proportional to $2z^2 - r^2$ and a homogeneous magnetic field) when $\mathbf{F} = 0$. When $\mathbf{F} = 0$, $\mathbf{r}_+$ and $\mathbf{r}_-$ are constant magnitude vectors rotating in the direction which is left-hand circular, with respect to the magnetic field, with frequencies equal to ω_+ and ω_-, respectively. For the purpose of this work, it is convenient to combine the electric field derived from the quadrupolar trap potential with $\mathbf{F}$, then Eqn (6) simplifies to

$$\frac{d\mathbf{r}_{cj}}{dt} = \left(\omega_{cj}\mathbf{r}_{cj} - \frac{\mathbf{E}_j}{B}\right) \times \hat{\mathbf{z}} \qquad (7a)$$

for the cyclotron position vector ($\omega_{cj} = q_j B/m_j$) and

$$\frac{d\mathbf{r}_{mj}}{dt} = \frac{\mathbf{E}_j}{B} \times \hat{\mathbf{z}} \qquad (7b)$$

for the magnetron (or guiding center) position vector, where $\mathbf{E}_j$ is the sum of the space charge electric field due to all other ion clouds and any externally applied electric field (e.g. excitation or trap electric fields) acting on the jth ion cloud. One should observe that if $\mathbf{E}_j$ in Eqn (7) includes the trap electric field then Eqn (7) is exact, being just an alternative set of coordinates to either Eqn (6) or the familiar Newton equation of motion with Lorentz force. The entire system of simultaneous first-order differential equations (4 × number of ion clouds) is integrated including explicitly the Coulomb interaction. The Coulomb electric field between cylindrical ion clouds whose centers are separated by distance r_{ij} is chosen such that the electric field is zero for complete overlap ($r_{ij} = 0$), increases linearly with separation distance up to the point where the ions clouds are just touching (at $r_{ij} = 2\rho_c$), then follows the usual line charge electric field dependence when the cylinders are completely separated ($r_{ij} > 2\rho_c$). This form of interaction electric field is most accurate for uniform charge density cylinders. Further details and discussion of this procedure are presented elsewhere.[11]

Each cloud's center position in the xy plane is $\mathbf{r}_j = \mathbf{r}_{cj} + \mathbf{r}_{mj}$, the sum of the cyclotron and magnetron position vectors. In order to integrate Eqn (7), a choice must be made for the coordinate representation of the cyclotron and magnetron position vectors. Cartesian coordinates are used for the magnetron position. However, two different representations are used here for the cyclotron position, either Cartesian or amplitude-phase (polar) coordinates, depending on the particular application. For problems where the initial cyclotron radius is zero, the equations of motion in Cartesian form are more appropriate. The amplitude–phase form of the equations of motion have a singularity in the phase equation at zero cyclotron radius and, therefore, are not easily applied to that situation. On the other hand, for problems where the initial cyclotron radius is not zero (e.g. after excitation), the amplitude–phase equations have a number of advantages including an accurate method for determining small changes in cyclotron frequency due to perturbations since the cyclotron phase is directly evaluated. With this numerical method the perturbed cyclotron frequency ($\omega_{cj} + \Delta\omega_{cj}$, where $\Delta\omega_{cj}$ is the frequency shift due to Coulomb interactions) is easily calculated for each ion cloud.[11] Phase locking between two ion clouds occurs when their perturbed cyclotron frequencies are equal. Both representations are described in detail elsewhere.[11]

If the magnetron and cyclotron equations of motion are both in Cartesian coordinates, the equations of motion are integrated by second-order central difference approximations. For example, the magnetron equation of motion $d\mathbf{r}_{mj}(t)/dt = \mathbf{E}_j(t)/B \times \hat{\mathbf{z}}$ is approximated by $[\mathbf{r}_{mj}(t + \delta t) - \mathbf{r}_{mj}(t - \delta t)]/2\delta t = \mathbf{E}_j(t)/B \times \hat{\mathbf{z}}$, where δt is the time step. This algorithm is stable for a sufficiently small time step and exhibits the time centering property which is important for good conservation of energy and angular momentum. As a partial test, the cyclotron motion of a single m/z 28 ion with a 1 cm cyclotron radius in a 1 T magnetic field was integrated for 10^5 cyclotron periods. With a time step equal to 1/300 of a cyclotron period, the cyclotron radius remained constant to within 1×10^{-3}. Using a time step six times larger, the cyclotron radius remained constant to within 5×10^{-3}. In cases where the cyclotron equation of motion is in amplitude–phase representation, the employed numerical integration method is the same as described in our earlier work.[11]

Rotating frame cloud trajectories

In order to depict the various kinds of dynamics that two Coulombically interacting ion clouds undergo as the ion population increases to the point of phase locking, we have carried out a number of numerical

simulations with realistic conditions and made movies of their trajectories in different frames of reference. The most appropriate is the frame rotating with the average cyclotron frequency of the two clouds. To accomplish this, Eqn (7) is first numerically integrated in the laboratory frame, then the laboratory frame trajectories are simply transformed to the rotating frame. The rotating frame representation of ICR trajectories has previously been employed in a study of single ion motion during linear dipolar excitation.[20] The parameters used in these first simulations are chosen to approximate the experimental conditions of Naito and Inoue.[8] Two cylindrical ion clouds ($\rho_c = 0.1$ cm, $L = 3.3$ cm), $q_1 = q_2 = e$, $m_1 = 27.9949$ u, $m_2 = 28.0313$ u, in a 1 T magnetic field are excited to a cyclotron radius of 1.0 cm by chirp excitation. The excitation frequency is downswept from 600 to 500 kHz in 150 μs with a maximum excitation electric field of 760 V m^{-1}. These excitation conditions give a post-excitation cyclotron radius of 1.00 cm for both ion clouds when Coulomb interactions are neglected, and no magnetron motion is excited. After excitation, the trajectory of each cloud is followed for 3.6 ms (about 2000 cyclotron periods). Since the ion clouds start at the origin, the Cartesian coordinate representation of Eqn (7) is chosen for these particular numerical simulations.

Figure 1 presents cloud trajectories (centers of each cloud) in the frame of reference rotating with the average unperturbed cyclotron frequency, $(\omega_{c1} + \omega_{c2})/2$ for the two cylindrical ion clouds described above. Since the difference in unperturbed cyclotron frequency (712 Hz) is much smaller than the average cyclotron frequency (~ 550 kHz), the frame rotating with the average cyclotron frequency is most appropriate for discerning features of the cloud trajectory arising from Coulombic effects between ion clouds. The ion clouds initially start with their centers at the trap origin, then are excited by chirp excitation to a coherent radius of ~ 1 cm. Only the post-excitation trajectory is plotted. Each box in Fig. 1 measures 3.5 cm across with the origin at the center. Each cloud has the same relative abundance and Fig. 1(a)–(d) depict post-excitation trajectories for four different simulation runs with the total number of ions increasing from 1×10^5 to 1.8×10^6 ions. The higher cyclotron frequency ion cloud (m_1) and lower cyclotron frequency cloud (m_2) are plotted as solid and broken lines, respectively. The arrows within each figure depict the direction which the clouds follow through time.

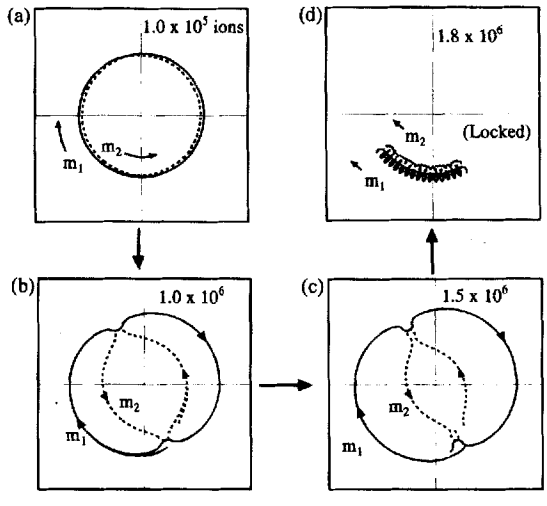

Figure 1. Post-excitation ion cloud trajectories in the *xy* plane, before and after cyclotron phase locking, in the frame of reference rotating with the average unperturbed cyclotron frequency. The faster (m_1) and slower (m_2) cloud center positions are plotted as solid and broken lines, respectively. The ion clouds have equal relative abundances. The axes are rotating frame coordinates. Four different ion populations are indicated: (a) 1×10^5, (b) 1×10^6, (c) 1.5×10^6 and (d) 1.8×10^6 ions. The ion clouds are phase locked at 1.8×10^6 ions. Parameters are $B = 1$ T, $m_1 = 27.9949$, $m_2 = 28.0313$, $q_1 = q_2 = e$, $L = 3.3$ cm and $\rho_c = 0.1$ cm. The ion clouds start initially overlapping at the trap center, then are excited by frequency sweep dipolar excitation from 600 to 500 kHz in 150 μs with an excitation electric field amplitude of 760 V m^{-1} (or 1520 V_{pp} m^{-1}). These trajectories result from numerical integration of Eqn (7) by central differences for ~ 2000 cyclotron periods using a constant time step of $\sim 1/300$ of a cyclotron period.

If Coulomb interactions are neglected, then the trajectories in this rotating frame are coincident circles with radii equal to the constant cyclotron radius (1 cm). The relative directions of the ion trajectories are left- and right-hand circular, with respect to the magnetic field (which is orthogonal to the plane of the figure), for the faster (m_1) and slower (m_2) ion clouds, respectively. As Coulomb interactions become increasingly important, the trajectories begin to distort from the unperturbed circular orbit in the rotating frame. Figure 1(a) demonstrates that for 1×10^5 ions the trajectories are no longer circular, with m_1 and m_2 possessing time-averaged cyclotron radii which are slightly greater than or less than the unperturbed radius of 1 cm. Observe that although the centers of the two clouds collide at two points per orbital period in the plotted trajectory, they never actually cross orbits (the slower cloud trajectory always remains within the faster cloud trajectory).

Increasing the total number of ions (N_t) by an order of magnitude to 1×10^6 [Fig. 1(b)] distorts the rotating frame orbits to an even greater extent from circular and that the largest distortions occur where the two clouds overlap. It is seen that the time-averaged cyclotron radius is enhanced and diminished, as the number of ions increases, for the higher and lower cyclotron frequency species. These trends are in agreement with previously published theory,[11] and with experimental data measuring relative ion abundances as a function of increasing ion population for two close masses.[7,12] The time-averaged cyclotron radius is essentially equal to the ion cloud distance from the trap center, averaged over the entire trajectory. The difference in time-averaged cyclotron radius between the higher and lower cyclotron frequency species arises from the additional cyclotron velocity perturbation in the $-\mathbf{E} \times \mathbf{B}$ direction.[11] Since the space charge electric fields are equal in magnitude and opposite in direction, simple geometry shows that m_1 is pushed to a larger cyclotron radius while m_2 is pushed to a smaller cyclotron radius.

Increasing N_t from 1.5×10^6 [Fig. 1(c)] to 1.8×10^6 ions [Fig. 1(d)] clearly shows that the trajectories are qualitatively different for those two cases. In Fig. 1(d) the two ion clouds have locked cyclotron modes. This is easily deduced from a number of perspectives. First, the maximum cloud separation distance is small compared with the cyclotron radius. The maximum separation distance is $\sim 2\rho_c$. The trajectory of one ion cloud never encircles the origin independent of the other cloud after

cyclotron phase locking. Finally, the two clouds oscillate many times in close proximity as compared with only two close collisions (in the rotating frame) for unlocked ion clouds. In the locked state the two clouds actually do not rotate completely around each other. After cyclotron phase locking, the Coulomb $\mathbf{E} \times \mathbf{B}$ drift entrains one ion cloud to the second cloud. However, the slower (m_2) and faster (m_1) clouds oscillate inwards and outwards, respectively, with respect to the trap center. This relative motion qualitatively resembles an antisymmetric normal mode oscillation since the ion clouds appear to move π out of phase with respect to each other. Although the centers of the two clouds completely overlap at closest approach, their orbits never cross, at least for the conditions used in our simulations. After the phase locking threshold has been surpassed, increasing the number of ions reduces the oscillation amplitude of relative motion and increases the Coulomb $\mathbf{E} \times \mathbf{B}$ oscillation frequency (proportional to E/B).

It is important to compare the numerical simulations with theoretical predictions for the number of ions required to lock cyclotron modes. Using the above parameters $B = 1$ T, $L = 3.3$ cm, $R_c = 1$ cm, $\rho_c = 0.1$ cm, $m = 28$ u and $\Delta m = 0.0364$ u in Eqn (2), we predict that $N_{max} = 1.7 \times 10^6$, in excellent agreement with the numerical result of 1.8×10^6 ions. Repeating the above numerical simulations with identical parameters except for doubling the excitation potential, thereby increasing the post-excitation cyclotron radius from 1 to 2 cm, we find that a minimum of 3.6×10^6 ions are required to lock cyclotron modes. This is in exact agreement with the theoretical prediction of Eqn (2) that N_{max} is directly proportional to R_c, not the R_c^3 dependence predicted by the recent theory of Naito and Inoue.[8]

Additional rotating frame trajectories, using the same experimental parameters as above, are presented in Fig. 2 to study the effect of varying relative ion abundance on the topology of the trajectories and on the phase locking threshold. The size of each box is the same as in Fig. 1, namely a width of 3.5 cm, and the ion clouds are excited to a coherent cyclotron radius of 1 cm. The upper and lower figures show trajectories before and after reaching cyclotron phase locking, respectively. Trajectories are presented for the two cases where the faster and slower ion clouds contain 90% of the total ion population, in the frame of reference rotating with the weighted mean unperturbed cyclotron frequency, i.e. the frame rotating with frequency $(N_1\omega_{c1} + N_2\omega_{c2})/N_t$, where $N_t = N_1 + N_2$. In Fig. 2(a) the higher cyclotron frequency cloud contains 90% of the ions, whereas in Fig. 2(b) the lower frequency cloud contains 90% of the total ion population. As expected, while both ion clouds are perturbed by the presence of the other, the most abundant ion cloud is much less affected. Although the number of ions required to lock cyclotron modes is different for the two relative abundances (also note from Fig. 1 that the case of equal relative abundance is intermediate), these differences are not very large, in agreement with Eqn (2). Also observe from the upper plots, corresponding to highly perturbed trajectories for the less abundant species close to phase locking, that the cyclotron trajectory is even more perturbed than for the case of equal relative abundance. The time-averaged cyclotron radius for the lower abundance species (which is approximately proportional to the detected FT-ICR signal) is greatly reduced or enhanced, just before cyclotron phase locking, depending on whether the less abundant species has a higher or lower mass, respectively, compared with the more abundant species. These trends are consistent with experimental observations.[12]

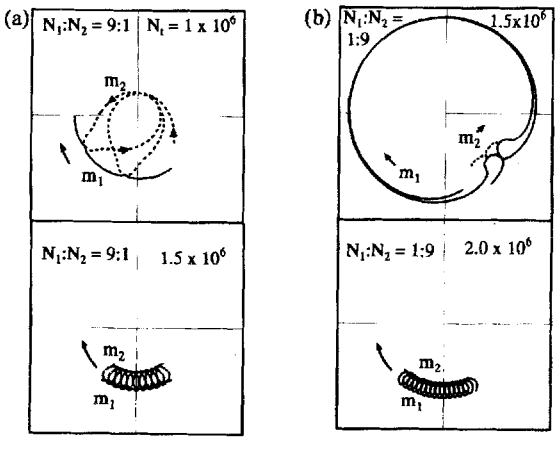

Figure 2. Post-excitation cloud trajectories in the xy plane, before and after cyclotron phase locking, for two different relative abundances of ions. (a) $N_1/N_2 = 9:1$, top $N_t = 1 \times 10^6$ and bottom $N_t = 1.5 \times 10^6$ ions; and (b) $N_1/N_2 = 1:9$, top $N_t = 1.5 \times 10^6$ and bottom $N_t = 2 \times 10^6$ ions. The ion clouds are phase locked in the lower plots. The other conditions are identical with those in Fig. 1.

Numerical calculation of rigid ion cloud phase locking thresholds

The previous discussion, with its use of the device of rotating frame ion trajectories, gives an insight into the kinds of motion two ion clouds with similar mass undergo as the ion population increases to the point of cyclotron phase locking. In order to test quantitatively the predictions of Eqns (2)–(4), the perturbed cyclotron frequencies are now calculated. A simple method to accomplish this accurately has already been developed and proven effective by numerically integrating Eqn (7) in Cartesian coordinates for the magnetron position and in amplitude–phase coordinates for the cyclotron position.[11]

As coordinates, we describe the position of each ion cloud by

$$x_j(t) = R_j \cos(\omega_{cj} t + \beta_j) + x_{mj}$$
$$y_j(t) = -R_j \sin(\omega_{cj} t + \beta_j) + y_{mj} \qquad (8)$$

where R_j, β_j, x_{mj} and y_{mj} are the cyclotron radius, cyclotron phase, magnetron x position and magnetron y position of the jth ion cloud, respectively. These four variables are obtained for each uniform charge density cylindrical ion cloud directly by numerical integration of the appropriate equations of motion.[11]

As a demonstration of cyclotron phase locking in two cylindrical ion clouds, Fig. 3 plots the perturbed cyclotron frequency of each ion cloud (relative to the weighted unperturbed cyclotron frequency $(N_1\omega_{c1} + N_2\omega_{c2})/N_t$) as a function of the total number of ions $N_t = N_1 + N_2$ for three different relative abundances. Figure 3(a), (b) and (c) are plots for relative ion abundances in the ratios of $N_1/N_1 = 1:1$, $9:1$ and $1:9$,

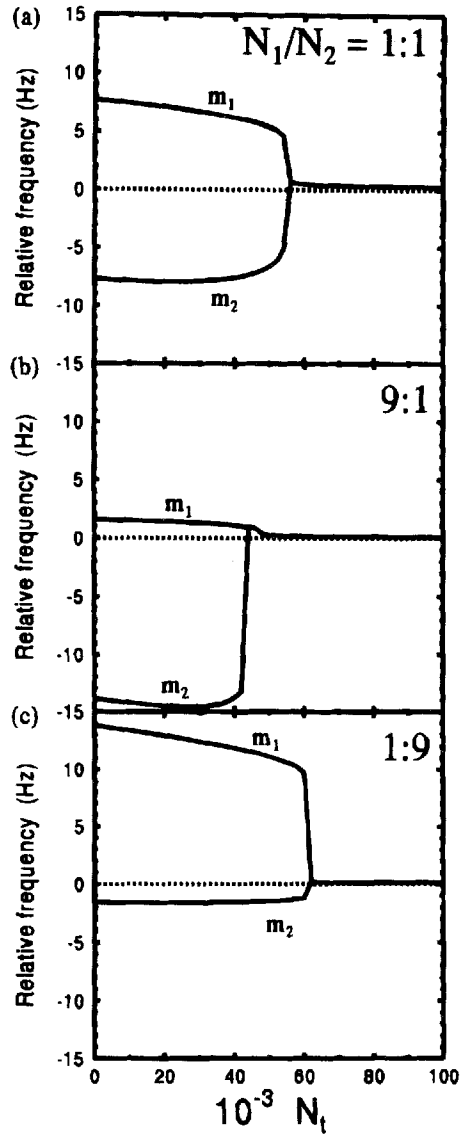

Figure 3. Numerical simulations of the approach to cyclotron phase locking for two cylindrical ion clouds. The perturbed cyclotron frequencies relative to the weighted mean unperturbed cyclotron frequency are plotted as a function of the total number of ions contained in the two clouds for three different relative ion abundances: N_1/N_2 ratios of (a) 1:1, (b) 9:1 and (c) 1:9. The ion clouds are started initially overlapping with equal cyclotron radii R_c and zero magnetron radii. The conditions include m_1 = 999 u, m_2 = 1000 u, $q_1 = q_2 = e$, B = 1 T, R_c = 1 cm, ρ_c = 0.1 cm and L = 5 cm.

respectively. The parameters used in the simulations include $m_1 = 999$ u, $m_2 = 1000$ u, $q = e$, $B = 1$ T and $L = 5$ cm. The clouds are started initially overlapping with $\beta_j = 0$ and $R_c = 1$ cm. Figure 3 shows that the ion clouds have different cyclotron frequencies with low ion population; however, as N_t increases past the phase locking threshold the cyclotron frequencies merge into a single collective cyclotron frequency which is approximately (but not exactly) equal to the weighted mean average of the unperturbed cyclotron frequencies.

Using these parameters, Eqn (2) predicts $N_{max} \approx 55 \times 10^3$ ions, in agreement with the numerical phase locking threshold of 56×10^3 ions in Fig. 3(a) for the case of equal abundance ion clouds ($N_1 = N_2$). Whereas Eqn (2) predicts that N_{max} is independent of the relative abundance of ions in each cloud, Fig. 3 shows that there is actually a relative ion dependence. The ratio of faster N_1 to the slower N_2 ion cloud in the ratios of 9:1 and 1:9 requires $\sim 42 \times 10^3$ and 62×10^3 ions to lock cyclotron modes. Additional theory (see Appendix) predicts that the fractional abundance dependence of N_{max} is given by Eqn (2) multiplied by an additional factor on the right which depends on the relative abundances and linearly on the ratio ρ_c/R_c.

Figure 4 compares results of numerical simulations for phase locking thresholds as a function of the fractional abundance of ions in the faster ($m_1 < m_2$) ion cloud, $f_1 = N_1/N_t$ (with $f_1 + f_2 = 1$). The numerical results are plotted as solid circles and the lines are used to depict the predominant linear dependence of N_{max} with fractional abundance. Two different initial cyclotron radii are shown, demonstrating good agreement between numerical simulations and analytical theory. The numerical simulations corroborate the prediction (see Appendix) that $dN_{max}/df_1 \propto -\rho_c^2$ although the predicted proportionality constant is smaller by a factor of ~ 1.7 compared with the numerical simulations. In the limit that $R_c \gg \rho_c$, Eqns (2)–(4) are the correct solutions for all relative abundances.

We next study the various parameter dependences predicted by Eqn (2) for the total number of ions required to lock two cylindrical ion clouds. N_t is varied in successive simulations with $N_1 = N_2$ until the perturbed cyclotron frequencies are equal. The solid circles in Fig. 5 are results from numerical simulations for the number of ions N_{max} required to lock cyclotron modes while the lines are predictions from Eqn (2). One observes very good agreement between analytical theory and numerical simulations for the conditions shown. In particular, the simulations agree with the prediction that $N_{max} \propto R_c\, \Delta m (B/m)^2$, independent of ionic charge for two ion clouds with the same charge state. Hence, it follows that $M_{max} \propto B(R_c\, \Delta m/N_{ave})^{1/2}$. These dependences also hold for spherical ion clouds (in the limit $R_c \ll \rho_c$), point charges ($R_c \gg s$) and line charges ($R_c \gg s$).

As a further test, phase locking involving more than two ion clouds is numerically investigated. Phase locking is studied in a model system representing cytochrome c ($M \approx 12 \times 10^3$ u). The nine most abundant

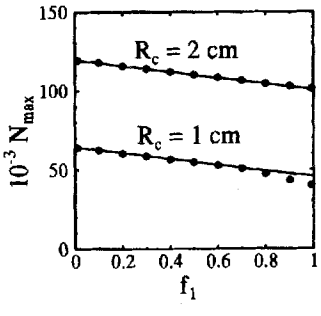

Figure 4. Results of computer simulations (solid circles) on the cyclotron phase locking thresholds for two cylindrical ion clouds as function of relative ion abundance. The lines are to demonstrate the predominant linear variation. There are $N_1 = f_1 N_t$ and $N_2 = f_2 N_t$ ions in clouds 1 and 2, respectively. Two different cyclotron radii are shown. Parameters include $q_1 = q_2 = e$, m_1 = 999 u, m_2 = 1000 u, B = 1 T, L = 5 cm and ρ_c = 0.1 cm. In the simulations the clouds are initially overlapping with cyclotron radius R_c.

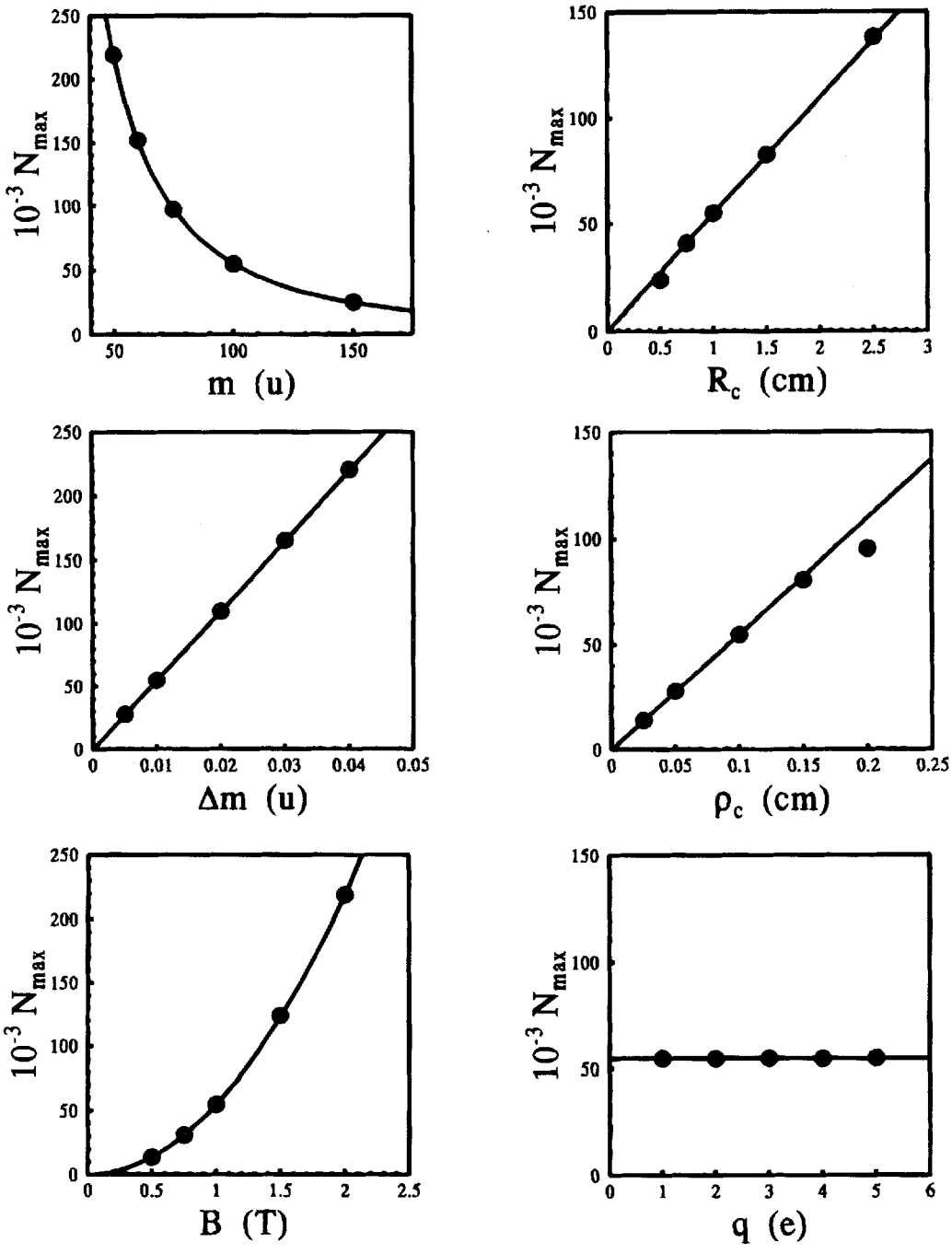

Figure 5. Numerical simulations (solid circles) compared with predictions of Eqn (2) (lines) for the number of ions contained in two ion clouds ($N_1 = N_2$ and $q_1 = q_2$) required to lock the cyclotron modes of two ion clouds. In the numerical simulations one parameter is varied at a time, keeping all others constant. The parameter values which remain constant have the values $m_1 = 99.99$ u, $m_2 = 100.00$ u ($\Delta m = 0.01$ u and $m = 100$ u), $B = 1$ T, $q = e$, $R_c = 1$ cm, $L = 5$ cm and $\rho_c = 0.1$ cm.

isotope peaks of either the 16+ or 4+ charge states of cytochrome *c* are included in the simulations. The relative abundances of the nine ion clouds from lowest to highest molecular mass are 35.8, 60.1, 83.1, 97.7, 100.0, 90.8, 74.1, 55.1 and 37.6. All ion clouds have the same dimensions ($\rho_c = 0.1$ cm, $L = 10$ cm) and start initially overlapping ($R_{c0} = 2.5$ cm, $\beta_{j0} = 0$) in a $B = 1$ T magnetic field. These initial conditions simulate ion clouds which extend the entire length of a 10 cm cubic trap and are excited to 50% of the maximum allowed radius. The number of ions in each cloud is varied in successive simulations while maintaining the correct relative abundances. Figure 6 plots the perturbed cyclotron frequencies (relative to the weighted average of the unperturbed cyclotron frequencies) and the maximum deviation in cyclotron radius from its initial value, ΔR_j, as a function of the number of ions N_0 in the most abundant isotope peak. The most abundant isotope is identified in Fig. 6 as the line closest to zero relative frequency. One observes that, as the number of ions increases, the most abundant isotope peak and its immediate neighbors lock first, although not simultaneously. Since the three central peaks in the isotope distribution are the most abundant, these isotopes lock

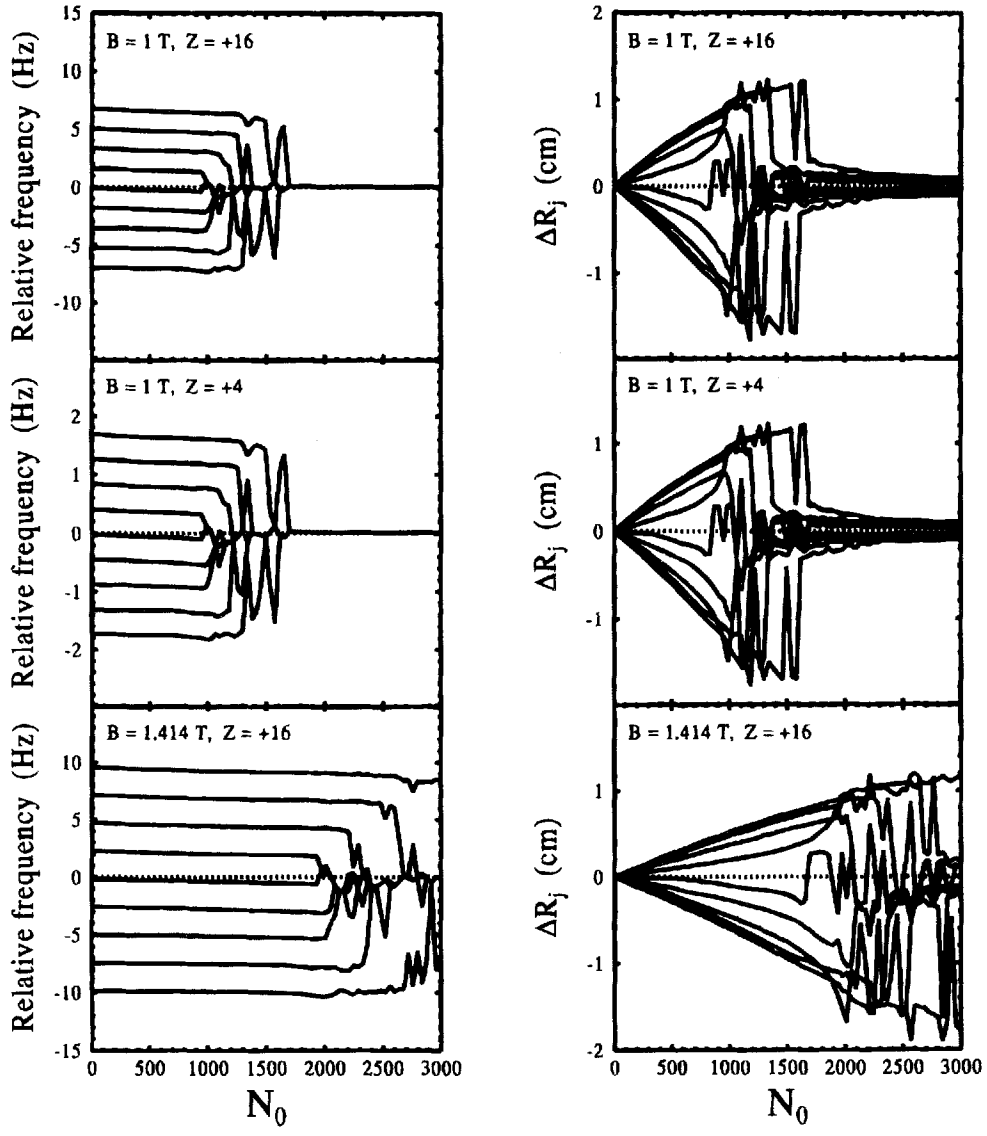

Figure 6. Numerical simulations of the approach to cyclotron phase locking for nine cylindrical ion clouds ($L = 10$ cm, $\rho_c = 0.1$ cm) with masses and relative abundances equal to the nine most abundant isotope peaks in cytochrome c ($M \approx 12\,000$ u). The perturbed cyclotron frequencies (relative to the weighted mean unperturbed cyclotron frequency) and maximum deviation in cyclotron radius are plotted as a function of the number of ions contained in the most abundant isotope peak. Top, $B = 1$ T, $z = 16+$; middle, $B = 1$ T, $z = 4+$; bottom, $B = 1.414$, $z = 16+$. The ion clouds are started overlapping with initial cyclotron radii $R_c = 2.5$ cm.

before the others. Two major trends are evident that are in agreement with the two ion cloud model, Eqn (2). The minimum number of ions required to lock two ion clouds (in this case the most abundant peak and one of its two closest neighbors lock first) is proportional to B^2 and is independent of the charge state. On going from the top to the middle of Fig. 6, which represents a reduction in charge state from $z = 16+$ to $z = 4+$, the number of ions required to lock the ion clouds (either the first two clouds to lock or all nine clouds to lock) is constant. In addition the ΔR_j plots are identical for these cases. On going from the top to the bottom of Fig. 6, the magnetic field increases from 1 to 1.414 T. The number of ions required to lock either the first two ion clouds or all of the ion clouds ($N_0 \approx 3400$, not shown) is doubled, in agreement with the predicted B^2 dependence of N_{max} for the two ion cloud model.

Since the most abundant isotope peaks have similar abundances, we make the approximation $N_0 \approx N_{max}/2$ in order to compare quantitatively with the predictions of the two ion cloud model. With $m = 12 \times 10^3$ u, $\Delta m = 1$ u, $L = 10$ cm, $R_c = 2.5$ cm, $\rho_c = 0.1$ cm and $B = 1$ T in Eqn (2) yields $N_{max}/2 = 950$, which is in very good agreement with $N_0 \approx 980$ ions required to lock the most abundant isotope peak of cytochrome c with a neighboring isotope peak.

Additional simulations were carried out to determine the influence of multiple charge states, which are trapped simultaneously, on the phase locking threshold for the isotopic envelope of each charge state. The five most abundant isotopes of both the $z = 4+$ and $z = 16+$ charge states of cytochrome c were included using the same experimental parameters as above. The isotopes in each charge state locked cyclotron modes with approximately the same number of ions as in identical simulations which retained only one of the two charge states. Hence, the presence of other charge states does not significantly influence the phase locking

threshold within a single charge state's isotopic envelope.

Full three-dimensional numerical simulations on realistic deformable ion clouds: removal of the rigid ion cloud assumption

Until now we have treated each m/z as a single rigid ion cloud with cylindrical shape. Inherent to this class of ion cloud are the assumptions that throughout the detection process, the ion cloud is stable and the density within each m/z cloud is nearly time independent. It is also possible that the Z-motion of ions within each cloud needs to be explicitly included in the analysis.

In order to address these issues, the two-dimensional rigid ion clouds are now generalized to full three-dimensional ion cloud models including internal ion cloud dynamics, non-quadrupolar trap potentials, linear dipolar excitation and Z-motion. All of the basic assumptions (and their possible effect on the validity of the rigid ion cloud model in relation to experimental results) contained in the rigid ion cloud model are removed, allowing for a stringent test of the earlier predictions.

The most important physical processes which limit the lifetime of coherent cyclotron motion are collisions with neutrals and position-dependent cyclotron frequencies arising from anharmonic trap potential, space charge effects and magnetic field inhomogeneities. In addition, an inhomogeneous dipolar excitation electric field reduces the cyclotron mode lifetime if the excitation event significantly distorts the ion cloud shape or reduces the number density. We shall demonstrate that, perhaps contrary to expectation, the long-range Coulomb interaction does not distort significantly the ion cloud during linear dipolar excitation.

Our three-dimensional model treats each different m/z ion cloud as a composite of a relatively large number of much smaller uniform density spherical ion clouds (i.e. superparticles) which have the same m/z as a single ion but charge of many ions. The motion of these superparticles is followed in three dimensions, including Coulombic interactions between superparticles of the same or different m/z and Z-motion in an applied trap electric field. While the individual superparticles have constant charge density (resulting in zero interaction force for two completely overlapping superparticles), there is no restriction on the charge density which the ion cloud can take. The distribution of superparticles is free to assume whatever charge density the equations of motion dictate.

The three-dimensional dynamic equations for the jth superparticle are given by Eqn (7) for the dynamics perpendicular to the magnetic field, supplemented by

$$\frac{dv_{zj}}{dt} = \left(\frac{q}{m}\right)_j \mathbf{E}_j \cdot \hat{\mathbf{z}}$$

$$\frac{dZ_j}{dt} = v_{zj} \tag{9}$$

for the parallel dynamics, where $\mathbf{E}_j \cdot \hat{\mathbf{z}}$ is the Z-component of the electric field (trap + Coulomb) and v_{zj} and Z_j are the Z-velocity and Z-position, respectively. The entire system of first-order differential equations (Eqns (7) and (9) for each superparticle, 6 × number of superparticles = 240 coupled differential equations) is integrated by second-order time-centered approximations with constant time step in Cartesian coordinates, as described before.

Initial distributions of superparticles, each with radius 0.1 cm, are generated to model approximately a 1 cm long, 0.1 cm radius cylindrical ion cloud which is initially aligned parallel to the magnetic field and trap Z-axis, by a selective cooling procedure. First, an initial ensemble of 40 superparticles is distributed by a random number generator to lie within a cylinder of length 1 cm along the Z-axis at the center of a specified trap potential. The superparticles are allowed to interact with each other via their Coulomb interaction and also with the applied electric and magnetic fields. Before cyclotron excitation, the positions of the individual superparticles within this distribution are followed for approximately 1 ms. During this time, a selective cooling procedure is implemented whereby any superparticles which have Z-positions exceeding ± 0.5 cm (i.e. that are outside of the desired ion cloud volume) have their Z-positions and Z-velocities reduced by half. This cooling method generates initial ensembles of superparticles which have the desired distribution ($\sim$1 cm long ion clouds in this case) and are in a quasi-equilibrium state (thermal equilibrium is not a requirement). Subsequently, the superparticles are followed in time to guarantee that the quasi-equilibrium state is reached, then are subjected to a linear dipolar chirp excitation of 0.15 ms duration to excite all ions to a 1 cm coherent cyclotron radius. The post-excitation trajectories of the superparticles are followed for up to 5000 periods of cyclotron motion.

As a first example, we study the 3D dynamics of 40 superparticles, each with radius 0.1 cm and m/z 100, as a function of the total number of ions (each superparticle represents a specified number of single ions with $q = e$ and m/z 100). Following the selective cooling procedure, the initial superparticle spatial distribution is in a quasi-equilibrium state which approximates a 1 cm long, 0.1 cm radius cylindrical ion cloud. The applied trap potential used in all of the 3D simulations is given by the cosh potential

$$\Phi_t(x, y, Z) = \frac{16V_t}{\pi^2 \cosh\left(\frac{\sqrt{2}\pi c}{2d}\right)} \cosh\left(\sqrt{2}\pi \frac{Z}{d}\right) \times \cos\left(\pi \frac{x}{d}\right)\cos\left(\pi \frac{y}{d}\right) \tag{10}$$

where V_t, c and d are the trap potential, trap length along the Z-axis, and trap width, respectively. The name cosh potential has previously been given for the special case of Eqn (10) along the Z-axis.[21] As parameters, we use $V_t = 3$ V and $c = d = 5$ cm (cubic cosh trap). This potential is simply the most important and lowest harmonic in the double Fourier series expansion of the exact tetragonal ICR trap potential. We have chosen to use the approximate cosh potential in the numerical simulations for convenience since this potential is much

faster to evaluate than the exact cubic trap potential. The basic physics is independent of the particular trap potential employed. Besides, the cubic cosh potential is actually more anharmonic than the true cubic potential. If the ion cloud is stable in the cosh potential, it certainly is stable in the true cubic potential. The cubic cosh potential is very well characterized and directly comparable to the exact cubic potential by expanding along the Z-axis in a Taylor series:

$$\Phi_t(Z) = V_t \sum_{n=0} D_{2n} \left(\frac{Z}{d}\right)^{2n} \tag{11}$$

The D_{2n} for the cubic cosh potential, up to fourth-order, are D_0 0.35, D_2 3.43 and D_4 5.64. These are to be compared with the true cubic trap coefficients D_0 0.33, D_2 2.77 and D_4 1.02. The relative anharmonicity (defined as the ratio D_4/D_2) is more than four times greater for the cosh potential than the true cubic potential.

Even in the absence of Coulomb interactions, trap potential anharmonicity (proportional to D_4 or higher) shifts the single ion cyclotron, magnetron and Z-oscillation frequencies from their quadrupolar values. In particular the fourth-order anharmonic potential changes the single ion cyclotron frequency from ω_+ to $\omega_+ + \delta\omega_c$, where $\delta\omega_c$ depends on the ion's position within the trap according to[22,23]

$$\delta\omega_c = \frac{3V_t D_4}{2Bd^4}(-2A_z^2 + 2R_m^2 + R_c^2), \tag{12}$$

where R_c, R_m and A_z are the ion's cyclotron radius, magnetron radius and Z-amplitude, respectively. Neglecting internal ion cloud Coulomb interactions, $\delta\omega_c$, ultimately limits the lifetime of coherent cyclotron motion by smearing the ion cloud over its cyclotron trajectory in a time $\sim 2\pi/\Delta\omega_c^{ext}$, where $\Delta\omega_c^{ext}$ is the maximum spread in cyclotron frequency across the ion cloud. One should note that magnetic field inhomogeneity and the Coulomb interaction from other m/z ion clouds are also important processes which give mode-amplitude dependent cyclotron frequencies. In this example, the spread in cyclotron frequency is due to trap potential anharmonicity according to Eqn (12). The maximum theoretical mass resolution[24] $R = 0.26qBT/m$, where T is the observation time, is $R \approx 1.6qB/(m\Delta\omega_c^{ext})$ if the observation time is equal to the coherence time. We now proceed to demonstrate that a sufficiently strong internal ion cloud Coulomb electric field negates this mechanism of cyclotron mode dephasing.

3D simulations on a single m/z deformable ion cloud

It is important to determine the combined effects of linear dipolar excitation and anharmonic trap potential on the shape of a realistic deformable single m/z ion cloud, since our rigid 2D ion cloud analysis assumes that the ion cloud shape and density are time invariant. In all of the 3D simulations we begin with a quasi-equilibrium ensemble of superparticles (constant charge density spheres of radius 0.1 cm) arranged initially along the Z-axis of a cubic cosh potential [Eqn (10) with $V_t = 3$ V and $c = d = 5$ cm]. A nominally 1 cm long, 0.1 cm radius ion cloud is prepared by selectively cooling a randomly chosen distribution of 40 superparticles. Each superparticle contains a 1750e charge with m/z 100 and, therefore, models a 1 cm long cylindrical ion cloud containing $40 \times 1750 = 70 \times 10^3$ singly charged m/z 100 ions. This ion cloud is initially aligned parallel to magnetic field ($B = 1$ T) at the center of the trap. After the cooling procedure, the superparticles are integrated in time for 1 ms, followed by a linear dipolar chirp excitation. The excitation frequency is swept from m/z 300 to 50 in 0.15 ms with an amplitude set to excite the cyclotron modes to 1 cm radius. The post-excitation superparticle trajectories are then followed for a relatively long detection period.

Figure 7 plots the superparticle distribution in the yZ plane at times corresponding to 0.3 ms before and 0.3 ms after the excitation event. The most important observation is that the linear dipolar excitation does not distort significantly this ion cloud from its original shape. Figure 8 shows superparticle Z-positions as a function of time for five representative particles in this distribution. The chirp begins at time $t = 0$ and lasts 0.15 ms. Afterwards, the superparticles have coherent cyclotron radii ~ 1 cm. Modulation of $Z(t)$ arising primarily from the strong Coulomb electric field is clearly evident in Fig. 8. The Coulomb interaction couples the Z-modes of all superparticles for these conditions resulting in Z-mode energy exchange. This energy exchange is reflected in Fig. 8 as the variation in modulation envelope of the different $Z_j(t)$. As an example, $Z_4(t)$ starts with approximately zero Z-amplitude (neglecting Coulomb interactions this particle remains close to the $Z = 0$ plane). However, by $t = 1.4$ ms, the Z-amplitude for this superparticle increases to ~ 0.5 cm, which is the length of the ion cloud.

Having demonstrated that the 3D ion cloud shape remains virtually invariant before and after linear dipolar excitation, we proceed to study the stability of coherent cyclotron motion. We have undertaken a series of numerical simulations to examine the effect of increasing the number of ions contained in the ion

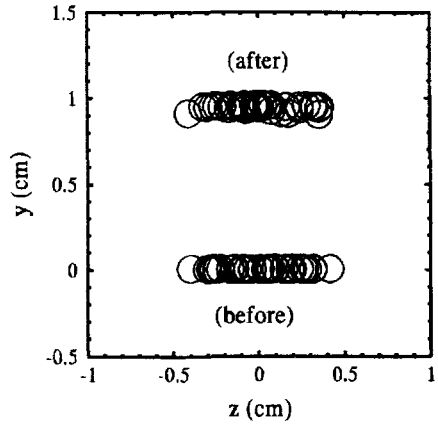

Figure 7. Superparticle yZ positions 0.3 ms before and 0.3 ms after the linear dipolar excitation event. The full 3D equations of motion are numerically integrated. A 1 cm long, 0.1 cm radius ion cloud consisting of 70×10^3 singly charged m/z 100 ions is modeled by 40 m/z 100 charged spheres (radii 0.1 cm) each carrying 1750e charge. The 0.15 ms chirp excitation event excites the cloud (originally along the z-axis) to $R_c \approx 1$ cm.

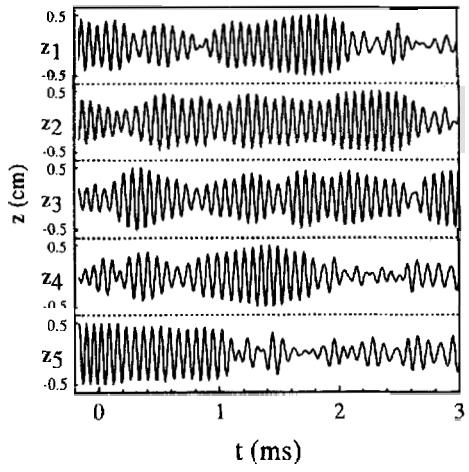

Figure 8. Z-Positions as functions of time for five out of 40 superparticles. Parameters as in Fig. 7. Since the superparticles approximate a 1 cm long cloud, a particle with $|Z(t)| = 0.5$ cm is at the cloud edge.

cloud. Figure 9 shows xy projections at 15.5 ms after the chirp excitation for different simulation runs, employing the same trap and cloud shape parameters as above except that the charge contained in each superparticle is varied in different runs while maintaining m/z 100. Figure 9(a)–(d) show the effect of increasing the total number of ions from zero (neglect of Coulomb interactions altogether) to 75×10^3 ions.

In the absence of Coulomb interactions [Fig. 9(a)], the ion cloud spreads out in an arc over its cyclotron trajectory. This smearing effect is due to the variation in cyclotron frequencies across the cloud arising from the anharmonic trap potential. The cyclotron frequency difference ($\Delta\omega_c^{ext}$) for this ion cloud can be estimated from Fig. 9(a) by dividing the arc length in radians of the cyclotron trajectory spread by time. Using this procedure, $\Delta\omega_c^{ext} \approx (2\pi)$ 36 Hz, indicating that the lifetime of coherent cyclotron motion ($T = 2\pi/\Delta\omega_c^{ext}$) is limited to 28 ms for this particular ion cloud, neglecting Coulomb interactions. The variation in cyclotron frequency, for this example, predominantly comes from the fourth-order anharmonic trap potential. From Eqn (12), $\Delta\omega_c^{ext} \approx |(\delta\omega_c(A_z = 0.005 \text{ m}) - \delta\omega_c(A_z = 0)| = (2\pi)$ 30 Hz, using the above parameters.

Coulomb interactions substantially influence the lifetime of coherent cyclotron motion. In Fig. 9(b), the total number of ions contained in the ion cloud is increased to 25×10^3. The ion cloud is even more distorted than when Coulomb interactions are neglected. Additional numerical simulations using 10×10^3 ions (not shown) show that internal cloud Coulomb interactions reduce the lifetime of coherent cyclotron motion by a factor of four times smaller compared with the case when Coulomb interactions are negligible [Fig. 9(a)]. However, in Fig. 9(c) and (d), corresponding to 50×10^3

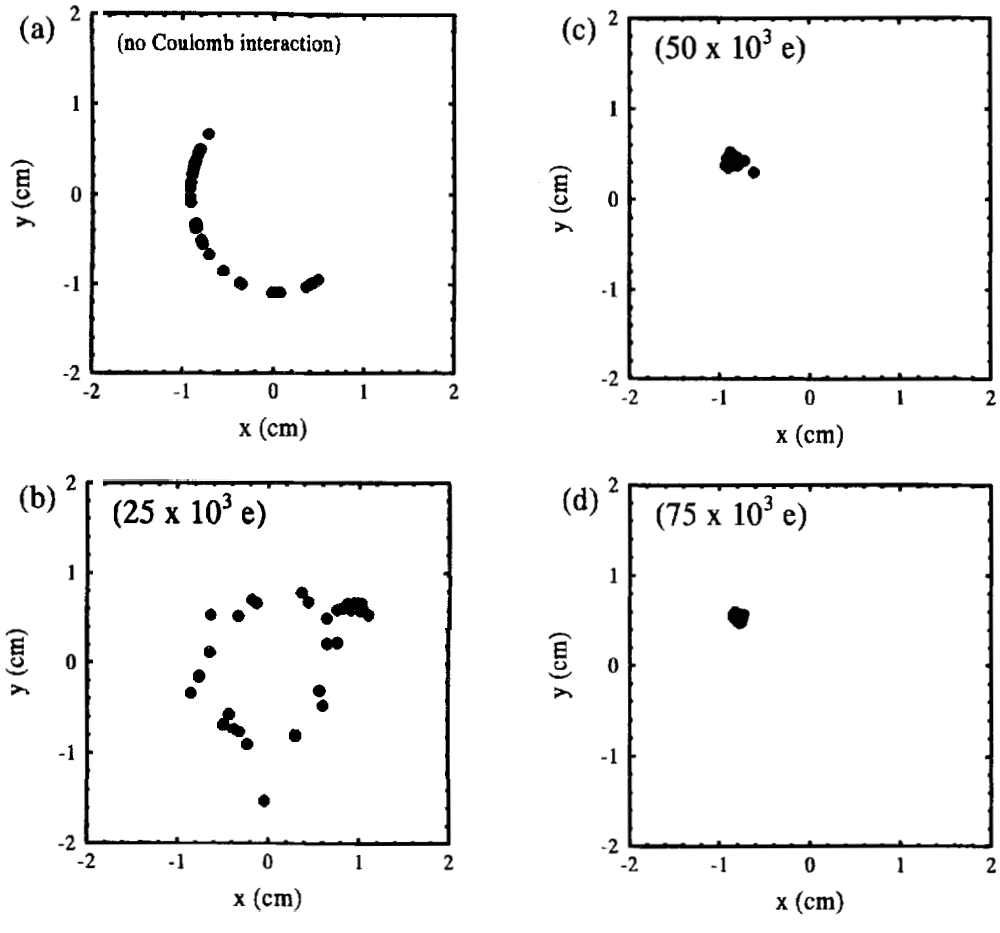

Figure 9. Rotating frame xy superparticle positions at 15.5 ms after excitation for an m/z 100 ion cloud modeled by 40 superparticles. (a) Neglect of Coulomb interactions; (b) $25 \times 10^3 e$; (c) $50 \times 10^3 e$; (d) $75 \times 10^3 e$ total charge.

and 75×10^3 ions, respectively, the ion cloud remains coherent, hence stable. Similar observations have been reported by Miluchihin *et al.*[25] on the basis of computer simulations. This phenomenon is completely analogous to cyclotron phase locking between different m/z ion clouds, except now the cyclotron frequency difference arises from the trap potential anharmonicity instead of a difference in m/z. The origin is due to a sufficiently strong internal ion cloud Coulomb $\mathbf{E} \times \mathbf{B}$ drift to overcome differences in cyclotron frequency across the cloud.[9] The internal ion cloud Coulomb $\mathbf{E} \times \mathbf{B}$ drift stabilizes the ion cloud for sufficiently strong electric field. On the other hand, as our simulations demonstrate, if this locking limit is not achieved, the Coulomb $\mathbf{E} \times \mathbf{B}$ drift may significantly reduce the lifetime of coherent cyclotron motion compared with the case when Coulomb interactions are neglected. For a single m/z cylindrical ion cloud which has a variation in cyclotron frequency at different positions across the cloud (e.g. as a result of trap anharmonicity or magnetic field inhomogeneity), according to Eqn (1), the ion cloud is stable provided that

$$\Delta\omega_c^{ext} < (0.050)\frac{Nq}{\varepsilon_0 BLR_c\rho_c} \tag{13}$$

The variation in cyclotron frequency across the ion cloud, $\Delta\omega_c^{ext}$, is due to any mechanism which gives rise to a spatially dependent cyclotron frequency. With $\Delta\omega_c^{ext} = (2\pi)$ 36 Hz, $q = e$, $L = 1$ cm, $B = 1$ T, $R_c = 1$ cm and $\rho_c = 0.1$ cm, Eqn (13) predicts that the internal Coulomb $\mathbf{E} \times \mathbf{B}$ drift stabilizes the ion cloud if $N > 25 \times 10^3$ ions. This estimate is in qualitative agreement with the 3D simulations which required 35×10^3 ions to stabilize the ion cloud. If the spread is cyclotron frequency is due to purely electrostatic processes, such as trap potential anharmonicity or Coulomb interactions, then $\Delta\omega_c^{ext} \propto B^{-1}$ (see Eqn (12), for example). Combining this magnetic field dependence with Eqn (13), we predict that the internal ion cloud phase locking condition to overcome the ion cloud smearing effect from electrostatic imperfections is independent of magnetic field. In spite of electric and magnetic field imperfections which limit the lifetime of coherent cyclotron motion, it is possible to overcome this limitation with a strong internal Coulomb $\mathbf{E} \times \mathbf{B}$ drift through the mechanism of cyclotron phase locking. This prediction pertains to achieving ultra-high resolution (i.e. 'infinitely long' coherent cyclotron motion), and not to the maximum possible resolution attainable if the locking condition, Eqn (13), is not satisfied, since maximum possible resolution $R \propto BT \propto B^2$ for electrostatic imperfections, neglecting Coulomb interactions.

The picture presented here is a follows: if the locking condition, Eqn (13), is not satisfied for a particular m/z ion cloud, then the cloud initially begins to spread in an arc over its cyclotron trajectory owing to cyclotron frequency differences arising from various external sources, most notably trap potential anharmonicity, magnetic field inhomogeneity and Coulomb interactions from other m/z ion clouds. Neglecting internal cloud Coulomb interactions, the lifetime of coherent cyclotron motion is $T \approx 2\pi/\Delta\omega_c^{ext}$. The maximum achievable mass resolution for this transient $R \approx (1.6)qB/(m\Delta\omega_c^{ext})$. Internal ion cloud Coulomb interactions dramatically alters these results. If the internal Coulomb $\mathbf{E} \times \mathbf{B}$ drift rotation is not strong enough to overcome variations in cyclotron frequency across the cloud, the ion cloud spreads in an arc in a time which can be much shorter than $2\pi/\Delta\omega_c^{ext}$. The origin of this Coulomb enhanced breakup of the ion cloud is not understood, though it may be related to the well known diocotron instability.[26] A diocotron mode is similar to the magnetron mode except the radial electric field arises from the image charge instead of the ICR trap. A single ion cloud which has a non-monotonic density distribution (e.g. a hollow beam or a partial annulus) is an unstable ion distribution which rapidly breaks apart, within the constraints of energy and angular momentum conservation.[26,27] This instability arises because an ion cloud which deviates significantly from circular cross-section (e.g. one which is partially smeared over its cyclotron trajectory) has significant variation in its internal $\mathbf{E} \times \mathbf{B}$ rotation frequency ($\propto \mathbf{E}/B$) across the cloud, resulting in shear which may destroy the cloud's coherence.

One interesting consequence of the diocotron instability to ICR relates to either creating ions off-axis by electron ionization[28] or injecting ions off-axis by an external source.[29] For these situations, the magnetron (or diocotron) motion rotates the ions during accumulation through an annulus resulting in a hollow density distribution (e.g. the ion cloud looks like a hollow cylinder in the xy plane with its center axis parallel to the Z-axis). A hollow beam distribution is unstable due to the diocotron instability, resulting in rapid breakup of this distribution and evolution towards a uniform distribution (some ions move towards the trap center while others move further away while conserving total canonical angular momentum[27] about the Z-axis). The diocotron instability has only been extensively studied for the low-frequency diocotron modes and not the high-frequency modes near the cyclotron frequency, although the stability results may carry over to both cases. Hence R is actually reduced from the zero Coulomb interaction prediction. On the other hand, if Eqn (13) is satisfied, then the strong internal Coulomb $\mathbf{E} \times \mathbf{B}$ rotation stabilizes the cloud, resulting in coherent cyclotron motion limited only by dissipative forces.

In the simulations presented here trap potential anharmonicity is dominant, which leads to a spatially dependent frequency given by Eqn (12) for the fourth-order trap potential. One should realize that trap potential anharmonicity is not the only mechanism which may lead to position-dependent cyclotron frequencies. Magnetic field inhomogeneity[30] or the Coulomb electric field[6] arising from other m/z ion clouds can also give non-zero $\Delta\omega_c^{ext}$. Even in the ideal case of ion motion in a purely quadrupolar (harmonic) trap potential and a homogeneous magnetic field, the Coulomb electric field from other m/z ion clouds give a non-zero $\Delta\omega_c^{ext}$.

An important result of the 3D numerical simulations for a single m/z is that in order to observe very long coherent cyclotron motion (say $>10^7$ cyclotron periods), the Coulomb $\mathbf{E} \times \mathbf{B}$ rotation within each m/z ion cloud must be sufficiently fast that the cloud does not break apart due to the cyclotron frequency variation across the cloud arising from applied fields. This conclusion supports earlier 2D stability model predic-

tions of Peurrung and Kouzes.[9] In the simulations, we distributed 40 superparticles of the same m/z within a cubic cosh potential (to produce a nominally 1 cm long, 0.1 cm radius cylindrical ion cloud), excited the superparticles to 1 cm cyclotron radius, and observed their behavior through time for a long post-excitation detection period. Since the approximate cubic cosh potential has a D_4 coefficient 5.5 times larger than the exact cubic potential, we predict that the same ion cloud requires just $N > 5 \times 10^3$ ions in an exact cubic potential (with 5 cm length and 3 V on the z-plates). One should realize that this prediction pertains to the achievement of infinitely long detected coherent cyclotron motion (pressure limited in practice) for an ensemble of ions with the same m/z, and not the minimum number of ions required to observe coherent cyclotron motion before the dephasing time $< 2\pi/\Delta\omega_c^{ext}$ is reached.

Prediction of an ultra-high resolution dynamic range limit for simultaneously confined species

As mentioned above, the Coulomb electric field arising from all other m/z ion clouds gives a non-zero frequency difference $\Delta\omega_c^{ext}$ across each ion cloud, which limits the lifetime of coherent cyclotron motion to $< 2\pi/\Delta\omega_c^{ext}$. In order to detect coherent cyclotron motion lasting $\gg 2\pi/\Delta\omega_c^{ext}$, the number of ions N in each m/z cylindrical ion cloud must be sufficiently high that Eqn (13) is satisfied. However, increasing N also increasing the Coulomb $\Delta\omega_c^{ext}$, making it more difficult to achieve stable coherent cyclotron motion. Furthermore, since the cyclotron frequency shift on cloud 1 due to the Coulomb electric field from cloud 2 is proportional to N_2, the number of ions in cloud 2, there is an ion abundance dependence to achieving stable coherent cyclotron motion. Our model predicts the existence of a maximum ultra-high resolution dynamic range due to the Coulomb frequency shift across the cloud.

Using Chen and Comisarow's estimate[6a] for the cyclotron frequency shift arising from a finite length line charge (cloud 2) on another line charge (cloud 1) [Eqn (19a) in Ref. 6a], the maximum variation in cyclotron frequency across cloud 1 is

$$\Delta\omega_{c1}^{ext} \approx \frac{\sqrt{2}N_2 q_2}{8\pi\varepsilon_0 B R_c^2}\left(\frac{1}{\sqrt{0.25L^2 + 2R_c^2}} - \frac{1}{\sqrt{L^2 + 2R_c^2}}\right). \tag{14}$$

where $\Delta\omega_{c1}^{ext}$ is the difference in cyclotron frequency between an ion in cloud 1 due to cloud 2 located at $Z = 0$ and an ion located at the cloud edge, $Z = L/2$. Combining Eqns (13) and (14) and then solving for the abundance ratio N_2/N_1 yields the condition for achieving 'infinitely long' transients (i.e. detected cyclotron motion lasting $\gg 2\pi/\Delta\omega_{c1}^{ext}$) for both m/z ion clouds:

$$\left(\frac{N_2}{N_1}\right)_{max} \approx 0.89\left(\frac{q_1}{q_2}\right)\left(\frac{R_c}{\rho_c}\right) \times \left[\frac{1}{\sqrt{0.25 + 2(R_c/L)^2}} - \frac{1}{\sqrt{1 + 2(R_c/L)^2}}\right]^{-1} \tag{15}$$

This equation should only be expected to give reasonable results when $L > 2\rho_c$, since the spread in cyclotron frequencies, Eqn (14), is derived for line charges. If $N_2/N_1 > (N_2/N_1)_{max}$, then Eqn (13) predicts that while cloud 2 is stable, the Coulomb electric field from cloud 2 on cloud 1 ultimately destabilizes cloud 1 in a time $< 2\pi/\Delta\omega_{c1}^{ext}$. Evidently, $(N_2/N_1)_{max}$ is an estimate of the maximum dynamic range for achieving simultaneous detected cyclotron motion lasting $\gg 2\pi\Delta\omega_c^{ext}$ in two different m/z ion clouds. As an example of the application of Eqn (15), if $q_1 = q_2$, $R_c = 1$ cm, $\rho_c = 0.1$ cm and $L = 1$ cm, then the maximum ultra-high resolution dynamic range $(N_2/N_1)_{max} \approx 100$. With $q_1 = q_2$, $R_c = 1$ cm, $\rho_c = 0.1$ cm and the limit $R_c \ll L$, then $(N_2N_1)_{max} \approx R_c/\rho_c = 10$. The maximum ultra-high resolution dynamic range is much higher for compressed ion clouds (just as long as the two clouds do not lock cyclotron modes). For example, if the two clouds are compressed to $L = 0.25$ cm, then $(N_2/N_1)_{max} \approx 4400$.

3D simulations on two closely spaced m/zs

We now describe the results of 3D simulations on two different m/z ion clouds (each m/z ion cloud is composed of 20 superparticles for a total of 40 superparticles). The same parameters are used in these simulations as above for the single m/z case. Each m/z ion cloud consists of 20 spherical superparticles of radius 0.1 cm. One ion cloud has m/z 100 while the second has m/z 100.15 u. The trap potential is the same as above, namely the cubic cosh potential with $V_t = 3$ V and $c = d = 5$ cm. Initial distributions of superparticles are generated by the selective cooling procedure to model nominally 1 cm long, 0.1 cm radius cylindrical ion clouds. The superparticles are excited by linear dipolar chirp excitation lasting 0.15 ms to yield a post-excitation cyclotron radius of 1 cm. Movies are created of the post-excitation trajectory, in the frame rotating with the weighted mean unperturbed cyclotron frequency.

Figure 10 plots the xy projection (perpendicular to B in the rotating frame) of superparticle positions at time $t = 2.1$ ms after excitation, which corresponds to the time $\pi/\Delta\omega_c$, where $\Delta\omega_c$ is the difference in unperturbed cyclotron frequency between the two ion clouds due to their mass difference. In Fig. 10(a) and (b) there are two distinct ion clouds corresponding to the two different m/zs. Each individual ion cloud is stable against the variation in cyclotron frequency arising from the trap potential anharmonicity (described above for the single m/z case), since the total number of ions in each cloud is greater than 35×10^3 (for a total of 70×10^3 in both clouds). However, the two different m/z ion clouds do not phase lock into a single cloud until the total number of ions in both clouds reaches 100×10^3, shown in Fig. 10(c). This phase locking threshold is directly comparable to analytical rigid ion cloud predictions. Putting $m = 100$ u, $\Delta m = 0.15$ u, $B = 1$ T, $R_c = 1$ cm, $L = 1$ cm and $\rho_c = 0.1$ cm into Eqn (2) gives the rigid ion cloud prediction that $N_{max} = 160 \times 10^3$ ions are required to phase lock the two different m/z ion clouds. The difference between the rigid ion cloud prediction and the 3D computer simulations on 40 superparticles may be attributed to the fact that the ion

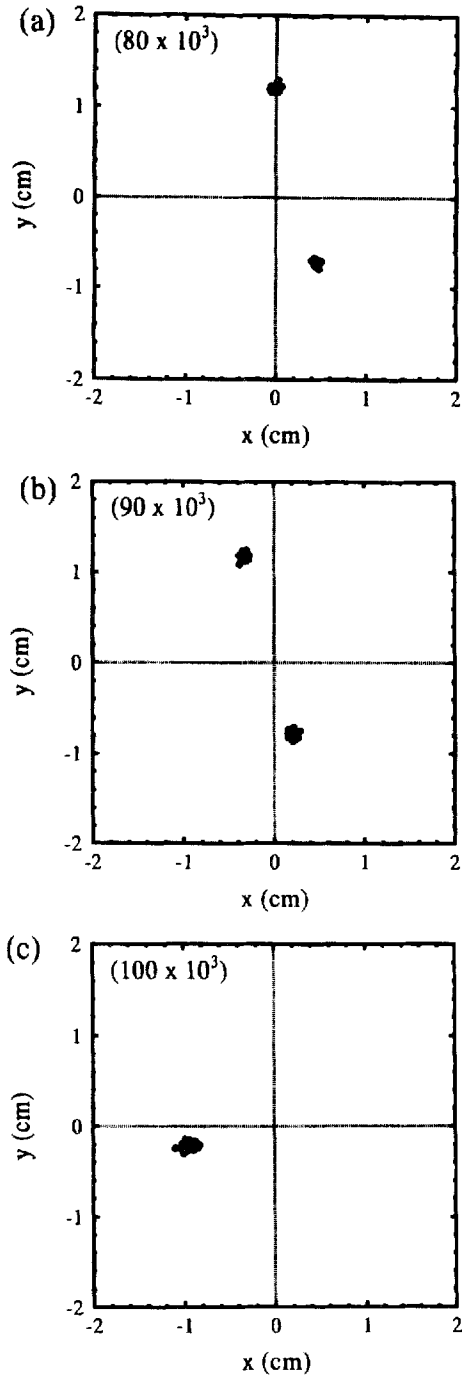

Figure 10. Rotating frame *xy* superparticle positions at 2.1 ms after cyclotron mode excitation for two different *m/z* ion clouds (100.00 and 100.15 u). The ion clouds are constructed out of 20 *m/z* 100.00 and 20 *m/z* 100.15 superparticles. The total charge contained in the two clouds is (a) 80×10^3 *e*, (b) 90×10^3 *e* and (c) 100×10^3 *e*. In (a) and (b) there are two distinct ion clouds, each with different *m/z*, whereas in (c) the two ion clouds have locked (coalesced) into a single cloud.

clouds used in the 3D simulations are not infinitely long charged cylinders but rather spheroidal. The ion clouds used in the 3D simulations actually have cloud length to radius ratios which place them between the two idealized cases of infinitely long cylinders and spheres. Previous rigid cloud studies have shown spherical ion clouds lock cyclotron modes with considerably fewer ions than very long clouds which have the same radius and total number of ions. From the perspective of mass spectrometry, Eqn (2) is actually a best case limit for the total number of ions required to lock cyclotron modes.

There are interesting implications to the dual requirements of achieving stable coherent cyclotron motion and preventing two closely spaced *m/z*s from locking cyclotron modes. In order to achieve stable coherent motion, one should increase the number of ions contained in the cloud. On the other hand, in order to prevent two closely spaced *m/z*s from locking cyclotron modes, the number of ions should be reduced. Therefore, the possibility exists that two closely spaced *m/z* ion clouds may lock cyclotron modes (i.e. coalesce into a single detected cyclotron frequency) with a smaller ion population than is required to stabilize the ion clouds. For this situation, the two ion clouds may be unresolvable regardless of the total ion population. In practice, the ion clouds may still be resolvable at low ion populations if the required mass resolution $m/\Delta m$ is considerably smaller than $\omega_c/\Delta\omega_c^{ext}$, where $\Delta\omega_c^{ext}$ is the variation in cyclotron frequency across a single *m/z* ion cloud due to field imperfections. The cloud stability limit, Eqn (13), applies towards the goal of achieving coherent cyclotron motion lasting $\gg 2\pi/\Delta\omega_c^{ext}$.

CONCLUSION

Analytical theory supported by numerical simulations demonstrates that the isotopic envelope is unresolvable past a high molecular mass limit (M_{max}) due to space charge induced cyclotron mode phase locking. M_{max} is proportional to B, independent of the charge state for ion clouds which are close in mass with equal charge state (e.g. the isotopic envelope for the molecular ions of a large biopolymer). M_{max} increases as $B\sqrt{\Delta m R_c/(\rho_c n_0)}$, where n_0 is the average number density (number of ions/cloud volume) for the two ion clouds, Δm is the mass difference and R_c/ρ_c is the cyclotron radius divided by the cloud radius.

These results should help serve as a guide in developing the next generation of ESI-FT-ICR mass spectrometers for high molecular mass applications. An order of magnitude estimate predicts that $M_{max} \approx 1 \times 10^4 B$ (in units of u and T), independent of charge state, for mass peaks which are 1 u apart. This estimate is consistent with present instrumental performance limits. While increasing an ion's charge state increases the achievable FT resolution (proportional to the cyclotron frequency and observation time of coherent cyclotron motion), M_{max} is unaffected by an increase in the ion's charge state. Once M_{max} has been surpassed, the isotopic envelope is unresolvable no matter how long the coherent motion is observed. The magnetic field strength and trap geometry (which is indirectly related to ion cloud shape and maximum allowed cyclotron radius) obviously should be chosen such that M_{max} is somewhat greater than the highest molecular mass system whose isotopic distribution is to be resolved.

The effects of internal ion cloud dynamics, *Z*-motion and anharmonic trap potential on cyclotron phase

locking have been studied by three-dimensional numerical simulations which treat every different m/z ion cloud as a relatively large number of Coulombically interacting superparticles. Each spherical superparticle has the same m/z as the ion cloud while containing the total charge and mass of many individual ions. The 3D simulations show that the shape of the ion cloud for a single m/z is virtually unaffected by linear dipolar excitation. Qualitatively, the full 3D simulations are consistent with the predictions of the 2D rigid ion cloud model. Also, there are actually two different phase locking conditions possible for realistic deformable ion clouds. For a single m/z ion cloud in a non-quadrupolar trap (i.e. in most real traps), there is a spread in cyclotron frequencies across the cloud as a result of frequency shifts arising from the anharmonic trap potential, magnetic field inhomogeneity or Coulomb electric field from other m/z ion clouds. For a sufficiently strong internal ion cloud Coulomb $\mathbf{E} \times \mathbf{B}$ rotation the different cyclotron frequencies, as a result of trap anharmonicity for example, lock into a single detected cyclotron frequency. In addition, the ion cloud remains coherent indefinitely. On the other hand, neglecting Coulomb interactions, the ion cloud smears out in an arc over its cyclotron trajectory in a time $\sim 2\pi/\Delta\omega_c^{ext}$, where $\Delta\omega_c^{ext}$ is the maximum variation in cyclotron frequency across the cloud arising from field imperfections. Even in the ideal case of ion motion in a purely quadrupolar (harmonic) trap potential and homogeneous magnetic field, the Coulomb electric field from other m/z ion clouds give a non-zero $\Delta\omega_c^{ext}$.

Analogously, the 3D simulations on two different closely spaced m/zs agree with the rigid ion cloud result for cyclotron phase locking due to m/z differences. A sufficiently strong Coulomb $\mathbf{E} \times \mathbf{B}$ rotation between the two different m/z ion clouds locks the cyclotron modes of the two ion clouds. The locking conditions in the full 3D simulations on realistic deformable ion clouds, including the effects of internal Coulomb interactions, Z-oscillation, linear dipolar excitation and trap potential anharmonicity, are in qualitative agreement with the predictions of the analytical 2D rigid ion cloud model.

There are two possible routes towards achieving ultra-high resolution by FT-ICR mass spectrometry. In the first approach, one simply goes to higher (and more expensive) magnetic fields, more ideal external fields and lower ion populations. The predictions of this work suggest an alternative route which should be used when the first approach fails and is especially relevant in low field instruments.

The first (or traditional) approach to achieving ultra-high resolution relies on increasing $\omega_c/\Delta\omega_c^{ext}$ to a level that the duration of coherent cyclotron motion is sufficient to resolve the species of interest. Increasing B increases mass resolution proportional to BT, where T is the observation time of coherent cyclotron motion.[1,24] From the viewpoint of this work, T is limited by differences in cyclotron frequency across the ion cloud to a maximum of $2\pi/\Delta\omega_c^{ext}$, neglecting Coulomb interactions. If $\omega_c/\Delta\omega_c^{ext}$ is made somewhat larger than $m/\Delta m$, then it is possible to observe coherent cyclotron motion long enough to reach the mass resolution $m/\Delta m$, regardless of the stability condition, Eqn (13). One still has to worry about locking cyclotron modes of closely spaced m/zs, but this can now be circumvented by reducing the ion density, according to Eqn (2) or (4). The difference in cyclotron frequency across the cloud, $\Delta\omega_c^{ext}$, can be reduced by making the ion cloud spatially more compact (owing to the positional dependence of the cyclotron frequency shifts arising from trap anharmonicity, Coulomb electric field and magnetic field inhomogeneity) and increasing B ($\Delta\omega_c^{ext} \propto B^{-1}$ for electrostatic imperfections). In addition, if a pure quadrupolar trap potential and homogeneous magnetic field are employed, trap potential anharmonicity and magnetic field inhomogeniety are eliminated, by definition, leaving just the Coulomb contribution to $\Delta\omega_c^{ext}$, which can be decreased by using smaller ion populations or higher B. This traditional approach may be the preferred direction towards the development of routine ultrahigh resolution performance since this approach involves minimal 'tuning.'

However, in the regime of low magnetic fields, for example, there is an alternative route towards achieving ultra-high resolution. There is also wide interest in the development of a low-field (low-cost) ultra-high resolution FT-ICR mass spectrometer for bench-top use or applications requiring portability.

The traditional route to ultra-high resolution fails if $m/\Delta m > \omega_c/\Delta\omega_c^{ext}$, because in this situation the coherent cyclotron motion dephases before a transient of sufficient duration can be acquired. In order to observe coherent cyclotron motion of an ion ensemble lasting much longer than $2\pi/\Delta\omega_c^{ext}$, it is necessary to stabilize the individual m/z ion clouds by increasing the ion density. Once stabilized, the 3D deformable ion clouds remain coherent indefinitely (pressure limited in practice). These stabilized ion clouds behave very similarly to rigid ion clouds. The predictions of this work are most relevant in the regimes of either ultra-high resolution, high ion population or low magnetic field. Basically, in order to achieve infinitely long coherent cyclotron motion, the ion population needs to be increased according to Eqn (13). However, increasing the number of ions to stabilize the individual m/z ion clouds also increases the likelihood that two closely spaced masses will lock cyclotron modes and coalesce into a single mass peak. Therefore, one should attempt to reduce $\Delta\omega_c^{ext}$ to acceptable levels by minimizing trap potential anharmonicity and magnetic field inhomogeneity. The contribution to $\Delta\omega_c^{ext}$ from the Coulomb electric field of other m/z ion clouds is still present and is predicted to give an upper dynamic range limit for simultaneously confined species varying from a low of $R_c/\rho_c \approx 10$, for ion clouds which are long compared with their cyclotron radii, to a dynamic range of several thousand for compact clouds. Although not investigated here, it is likely that dipolar excitation electric field inhomogeneity should be minimized in order to ensure that the ion cloud before and after dipolar excitation is in a quasi-equilibrium state and to minimize the cloud's post-excitation spatial extent, thereby minimizing $\Delta\omega_c^{ext}$.

The results of this work establish firm limits to performance that apply for conventional FT-ICR of high molecular mass species. As noted previously, FT-ICR performance degrades substantially as molecular mass increases, particularly in ESI owing to the combinatorial explosion of charge states and the size of the

isotopic envelope (and also practical limitations due to sample heterogeneity and adduction). These considerations require the use of larger ion populations in order to obtain a statistically representative sample, aggrevating the difficulties due to cyclotron phase locking. We note that one way to avoid the M_{max} limit described in this paper is to make measurements under conditions where resolution *per se* is not required. In fact, this laboratory has previously reported on individual ion methods that do this, and we have shown that molecular mass measurements for very large ions become possible.[31] A similar approach can also be proposed in which large numbers of spectra obtained with small ion populations are summed so as to circumvent the limit described. The practicality of such an approach remains to be established and at present the limitations described in this paper should be firm for conventional methodologies.

Acknowledgement

We thank Drs. Alan Rockwood and Tony Peurrung for useful discussions. This work was supported by Laboratory Directed Research and Development through the US Department of Energy. Pacific Northwest National Laboratory is operated by Battelle Memorial Institute through Contract No. DE-AC-0676-RLO-1830.

REFERENCES

1. A. G. Marshall and F. R. Verdun, *Fourier Transforms in NMR, Optical and Mass Spectrometry: A user's Handbook*. Elsevier, Amsterdam (1990).
2. F. W. McLafferty, *Acc. Chem. Res.* **27**, 379 (1994).
3. Q. Wu, S. Van Orden, X. Cheng, R. Baktiar and R. D. Smith, *Anal. Chem.* **67**, 2498 (1995).
4. J. P. Spier, M. W. Senko, D. P. Little, J. A. Loo and F. W. McLafferty, *J. Mass Spectrom.* **30**, 39 (1995).
5. S. Guan and A. G. Marshall, *Int. J. Mass Spectrom. Ion Processes* **146/147**, 261 (1995).
6. S. P. Chen and M. B. Comisarow, *Rapid Commun. Mass Spectrom.* (a) **5**, 450 (1991); (b) **6**, 1 (1992).
7. G. T. Uechi and R. C. Dunbar, *J. Am. Soc. Mass Spectrom.* **3**, 734 (1992).
8. Y. Naito and M. Inoue, *J. Mass Spectrom. Soc. Jpn.* **42**, 1 (1994).
9. A. J. Peurrung and R. T. Kouzes, *Phys. Rev. E* **49**, 4362 (1994).
10. A. J. Peurrung and R. T. Kouzes, *Int. J. Mass Spectrom. Ion Processes* **145**, 139 (1995).
11. D. W. Mitchell and R. D. Smith, *Phys. Rev. E* **52**, 4366 (1995).
12. J. Huang, P. W. Tiedemann, D. P. Land, R. T. McIver and J. C. Hemminger, *Int. J. Mass Spectrom. Ion Processes* **134**, 11 (1994).
13. L. Paša-Tolić, Y. Huang, S. Guan, H. S. Kim and A. G. Marshall, *J. Mass Spectrom.* **30**, 825 (1995).
14. E. Sarid, F. Anderegg and C. F. Driscoll, *Phys. Plasmas* **2**, 2895 (1995).
15. J. J. Bollinger, D. J. Wineland and D. H. E. Dubin, *Phys. Plasmas* **1**, 1403 (1994).
16. M. D. Tinkle, R. G. Greaves, C. M. Surko, R. L. Spencer and G. W. Mason, *Phys. Rev. Lett.* **72**, 352 (1994).
17. E. N. Nikolaev, N. V. Miluchinin and M. Inoue, *Int. J. Mass Spectrom. Ion Processes* **148**, 145 (1995).
18. T. Solouki, K. J. Gillig and D. H. Russell, *Anal. Chem.* **66**, 1583 (1994).
19. L. Brillouin, *Phys. Rev.* **67**, 260 (1945).
20. M. Wang and A. G. Marshall, *Int. J. Mass Spectrom. Ion Processes* **100**, 323 (1990).
21. S. A. Hofstadler and D. A. Laude, *J. Am. Soc. Mass Spectrom.* **1**, 351 (1990).
22. D. W. Mitchell, *Int. J. Mass Spectrom. Ion Processes* **142**, 1 (1995).
23. M. Kretzschmar, *Phys. Scr.* **46**, 544 (1992).
24. A. G. Marshall, M. B. Comisarow and G. Parisod, *J. Chem. Phys.* **71**, 4434 (1979).
25. N. V. Miluchihin, K. Miura and M. Inoue, *Rapid Commun. Mass Spectrom.* **7**, 966 (1993).
26. T. M. O'Neil and R. A. Smith, *Phys. Fluids B* **4**, 2720 (1992).
27. T. M. O'Neil, *Phys. Fluids* **23**, 2216 (1980).
28. R. Chen and A. G. Marshall, *Int. J. Mass Spectrom. Ion Processes* **133**, 29 (1994).
29. S. Guan, L. Paša-Tolić, A. G. Marshall and X. Xiang, *Int. J. Mass Spectrom. Ion Processes* **139**, 75 (1994).
30. D. W. Mitchell, A. L. Rockwood and R. D. Smith, *Int. J. Mass Spectrom. Ion Processes* **141**, 101 (1995).
31. (a) R. D. Smith, X. Cheng, J. E. Bruce, S. A. Hofstadler, G. A. Anderson and R. D. Smith, *Nature (London)* **369**, 137 (1994); (b) J. E. Bruce, X. Cheng, R. Baktiar, Q. Wu, S. Van Orden, G. Anderson and R. D. Smith, *J. Am. Chem. Soc.* **116**, 7839 (1994); (c) R. Chen, Q. Wu, D. W. Mitchell, S. A. Hofstadler and R. D. Smith, *Anal. Chem.* **66**, 3964 (1994); (d) R. Chen, X, Cheng, D. W. Mitchell, S. A. Hofstadler, Q. Wu, A. L. Rockwood, M. G. Sherman and R. D. Smith, *Anal. Chem.* **67**, 1159 (1995).

APPENDIX

Test charge interacting with a non-perturbable cylindrical ion cloud with a coherent cyclotron mode

The cyclotron dynamics of a single test charge (or a line charge containing just one ion) which interacts with an infinitely long charged cylinder, containing a total charge much greater than the single test charge, represents the idealized case where the cyclotron motion of the charged cylinder is unperturbed by the test charge. While the test charge is perturbed by the cylinder's space charge electric field, the charged cylinder is virtually unaffected by the presence of the line charge. It follows from the magnetron mode equation of motion, Eqn (7b), that a single ion within the cylinder, before cyclotron excitation, rotates about the cylinder's own symmetry axis owing to the radial space charge electric field with frequency $\omega_r = E/Br$. Constant density ellipsoidal clouds in a homogeneous magnetic field rotate as rigid rotors without shear since their electric field is proportional to r within the ellipsoid. The constant density, rigid ion cloud assumption does not correspond to most ion clouds in ICR experiments since such density profiles occur only for ion clouds in the zero temperature high density limits.[15,16] For ion clouds which are in thermal equilibrium and have non-zero temperature, the density falls to zero at the cloud edge in a distance

on the order of the Debye length.[15,16] However, the constant density, rigid ion cloud assumption allows for relatively simple analytical predictions. In any case, we have shown that full three-dimensional numerical simulations on realistic ion clouds (non-zero temperature, variable density) give phase locking predictions in qualitative agreement with the rigid cloud model.

As an example, ω_r for an infinitely long cylinder of radius ρ_c and line charge density Nq/L (total charge Nq contained in a segment of the cylinder L long) is

$$\omega_r = \frac{Nq}{2\pi\varepsilon_0 \rho_c^2 LB} \quad \text{(cylindrical cloud)} \qquad \text{(A1)}$$

The most appropriate frame of reference for viewing a test line charge interacting with a non-perturbable ion cloud is the frame rotating with the ion cloud with origin at the cloud center. This rotating frame is illustrated in Fig. A1. The coordinates x_{lab} and y_{lab} are trap-centered coordinates in the laboratory frame, while x and y are cloud-centered coordinates in the rotating frame. Defining $\mathbf{r}_0$ and $\mathbf{r}_1$ as cyclotron position vectors in the laboratory frame with origin at the trap center for the ion cloud with cyclotron frequency ω_{c0} and test ion with cyclotron frequency ω_{c1}, respectively, the equations of motion in the laboratory frame, derived from Eqn (7a), are

$$\dot{\mathbf{r}}_0 = \omega_{c0}\mathbf{r}_0 \times \hat{\mathbf{z}}$$

$$\dot{\mathbf{r}}_1 = \omega_{c1}\mathbf{r}_1 \times \hat{\mathbf{z}} - \omega_r\left(\frac{\rho_c}{r}\right)^p(\mathbf{r}_1 - \mathbf{r}_0) \times \hat{\mathbf{z}} \qquad \text{(A2)}$$

where r is the distance from the ion cloud's symmetry axis to the test charge and p is an exponent dependent upon the assumed interaction. In particular, $p = 0$ within the cylinder ($r < \rho_c$) and $p = 2$ outside the cylinder ($r > \rho_c$). These choices for exponent are exact for a uniform charge density infinitely long cylinder of radius ρ_c. For this case, the space charge electric field is zero along the cylinder's axis ($r = 0$), increases linearly with r up to the cylinder's edge at $r = \rho_c$, then falls as $1/r$ for $r > \rho_c$. Transforming to a frame of reference rotating with the ion cloud and origin at the cloud's center

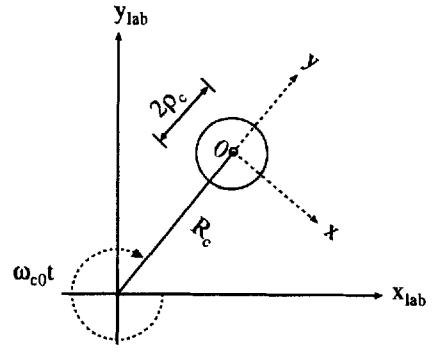

Figure A1. Frame of reference rotating with the ion cloud with frequency ω_{c0} and origin at the cloud center. The laboratory frame (origin at the trap geometric center) coordinates are x_{lab}, y_{lab} while the test ion is located at x, y in the rotating frame of reference. R_c and ρ_c are the cyclotron radius and cloud radius, respectively.

results in a single equation for the test ion:

$$\dot{\mathbf{r}}^* = \left[\Delta\omega_c - \omega_r\left(\frac{\rho_c}{r}\right)^p\right]\mathbf{r}^* \times \hat{\mathbf{z}} + \Delta\omega_c \mathbf{r}_0^* \times \hat{\mathbf{z}} \qquad \text{(A3)}$$

where $\Delta\omega_c = \omega_{c1} - \omega_{c0}$ and $\mathbf{r}^*$ is the test ion position vector in the rotating frame with origin at the cloud's center ($\mathbf{r} = \mathbf{r}_1 - \mathbf{r}_0$, $|\mathbf{r}| = |\mathbf{r}^*|$). In the rotating frame, the ion cloud position vector $\mathbf{r}_0^*$ is constant. Using Cartesian coordinates with the ion cloud along the y-axis,

$$\dot{x} = \left[\Delta\omega_c - \omega_r\left(\frac{\rho_c}{r}\right)^p\right]y + \Delta\omega_c R_c$$

$$\dot{y} = -\left[\Delta\omega_c - \omega_r\left(\frac{\rho_c}{r}\right)^p\right]x \qquad \text{(A4)}$$

By scaling time with the cloud rotation period $2\pi/\omega_r$ and length by R_c, these equations simplify to a non-dimensional form depending only on two parameters; ρ_c/R_c and $\Delta\omega_c/\omega_r$. For the case when an ion is not phase locked to the cloud, the test ion revolves completely around the trap center owing to the relative cyclotron motion in perturbed cyclotron orbits. One can show either analytically by a fixed point analysis (setting all time derivatives equal to zero then solving for the stability points with $p = 2$, which assumes that the test ion is initially located on the cloud edge) or by direct numerical integration that the phase locking condition predicted by Eqn (A4) for the test ion is different for the two cases $\Delta\omega_c > 0$ and $\Delta\omega_c < 0$. If $\Delta\omega_c > 0$, the test ion is bound to the ion cloud when

$$|\Delta\omega_c| < k^*\omega_r\left(\frac{\rho_c}{R_c}\right)\left(1 + \frac{\rho_c}{R_c}\right)^{-1} \qquad \text{(A5)}$$

where k^* is a constant whose value depends only on the cloud geometry and the initial position of the test charge within the ion cloud. The particular value for k^* can be deduced either from numerical simulations of Eqn (A4) or by comparison with Eqn (1). On the other hand, when $\Delta\omega_c < 0$, the stability condition is

$$|\Delta\omega_c| < k^*\omega_r\left(\frac{\rho_c}{R_c}\right)\left(1 - \frac{\rho_c}{R_c}\right)^{-1} \qquad \text{(A6)}$$

The test ion is more likely to be bound to the ion cloud when $\Delta\omega_c < 0$ (i.e. the test ion has a cyclotron frequency smaller than that of the ion cloud) than when $\Delta\omega_c > 0$. The reason why the sign of $\Delta\omega_c$ is involved in the phase locking threshold is that the test charge receives a Coulomb $\mathbf{E} \times \mathbf{B}$ velocity perturbation whose direction is either radially inward or outward from the cloud center depending on whether the test ion is moving faster or slower relative to the ion cloud.[11]

Now, consider two ion clouds with equal cloud dimensions but variable relative ion populations; Nq is replaced by $N_1q_1 + N_2q_2$ in Eqn (A1). In particular, cloud 1 contains f_1N_t while cloud 2 contains f_2N_t ions, where f_1 and f_2 are the relative fraction of the total number of ions N_t in each cloud ($f_1 + f_2 = 1$). Also, the unperturbed cyclotron frequency of ion in cloud 1 is assumed greater than that for cloud 2; therefore,

$m_1 < m_2$. Using these conventions, we propose that the locking threshold Eqn (2) is in the correct form for arbitrary relative ion abundances provided that the right-hand side of Eqn (2) is multiplied by the additional factor $1 + \rho_c/R_c(f_2 - f_1)$. This choice satisfies three basic limits: if (i) $f_1 = 0, f_2 = 1$, or (ii) $f_1 = 1, f_2 = 0$ or (iii) $f_1 = f_2 = 0.5$, then Eqns (A5), (A6) and (2), respectively, are recovered. Combining this proposed abundance dependence with Eqn (2) yields the minimum total number of ions to lock the cyclotron modes of two cylindrical ion clouds with a variable relative abundance of ions in each cloud ($f_1 + f_2 = 1, m_1 < m_2$):

$$N_{max} \approx 20.5\left(\frac{\varepsilon_0 L R_c \rho_c B^2 \Delta m}{m^2}\right)\left[1 + \frac{\rho_c}{R_c}(f_2 - f_1)\right] \tag{A7}$$

In the limit $R_c > > \rho_c$, Eqn (A7) reduces to Eqn (2) which is independent of the relative abundance. These trends agree with our numerical simulations and with previously published experimental data.